ABSTRACT

Title of Thesis: A CONTROL-THEORETIC MODEL OF HEMODYNAMIC RESPONSES TO BLOOD VOLUME PERTURBATION

Alex Kai-Yuan Lo, Master of Science, 2018

Thesis directed by: Associate Professor Jin-Oh Hahn
Department of Mechanical Engineering

This thesis presents a mathematical model to reproduce hemodynamic responses of different endpoints to the blood volume perturbation in circulation system. The proposed model includes three sub-models, which are a control-theoretic model relating blood volume response to blood volume perturbation, a physiologic-based model relating cardiac output response to blood volume perturbation, and a control-theoretic model relating mean arterial pressure response to cardiac output perturbation. Two unique characteristics of this hemodynamic model are that the model can reproduce responses accurately even with its simplicity, and can be easily understood by control engineers because of its physiological transparency. With these two advantages, closed-loop resuscitation controller evaluation can be performed in model-based approach instead of evaluating results from animal studies, which are relatively costly and time-consuming. In this thesis, the hemodynamic model was examined and evaluated by using experimental dataset collected from 11 animals. The results of system identification analysis, in-silico evaluation and parametric sensitivity analysis showed

that the hemodynamic model may faithfully serve as a evaluation basis for the closed-loop resuscitation controllers.

A Control-Theoretic Model of Hemodynamic Responses to Blood Volume Perturbation

By

Alex Kai-Yuan Lo

Thesis submitted to the Faculty of the Graduate School of the
University of Maryland, College Park in partial fulfillment
of the requirements for the degree of
Master of Science
2018

Advisory Committee:
Associate Professor Jin-Oh Hahn, Chair/Advisor
Professor Nikhil Chopra
Professor Miao Yu

Acknowledgments

I owe my gratitude to all the people who have help me make this thesis possible and whom I met in my journey of graduate endeavor.

First, I would like to thank my advisor, Dr. Hahn, for giving me a precious opportunity to work with him in his lab. His generous support and guidance have equipped me with valuable research skills and broaden my vision in the fields of system control and modeling. Besides, I am grateful that he has always been patient and guided me to the right way when I have difficulties in my research. I hope that my work in these two years can help Dr. Hahn and the other members in the lab move further in the future.

Besides, I would also like to thank my colleague members at the lab, especially the senior members, Xin Jin and Ramin Bighamian. They always help me to get familiar with the different concepts in the project and share plenty of useful ideas which help me move forward in the project.

In addition, I would also be grateful to Dr. Kramer who generously shared the experimental data of his study to us for model evaluation. This thesis would not have been possible without this invaluable animal dataset.

I also thank Dr. Chopra and Dr. Yu for being my thesis defense committee and providing me feedback of my thesis. I truly appreciate your time and consideration on evaluating my work.

I also appreciate the support from the Office of Naval Research (ONR) under Grant No. N000141410591 and N000141512018. This thesis can be possible because

of their funding.

In the end, I want to thank my family, especially my parents and my little aunt. Although they have not been with me at University of Maryland, they still always stand by my side and support me whatever decision I made. Without them, I cannot pursue my dream in the U.S.

Table of Contents

List of Tables

List of Figures

List of Abbreviations

AICc	Corrected Akaike information criterion
ARS	Acceptance-rejection sampling method
BV	Blood volume
CO	Cardiac output
CVP	Central venous pressure
DIV	Divergence
GSA	Global sensitivity analysis
HR	Heart rate
ICG	Indocyanine green dye
ISF	Interstitial fluid
LR	Lactated Ringer's solution
LSA	Local sensitivity analysis
LV	Left ventricular
LVEDP	Left ventricular end diastolic pressure
LVEDV	Left ventricular end diastolic volume
MAP	Mean arterial pressure
MC	Monte Carlo estimator
MDAPE	Median absolute prediction error
MDPE	Median prediction error
MSP	Mean systemic pressure
NRMSE	Normalized RMSE
OAT	One-at-a-time
pdf	Probability distribution function

RBCV	Red blood cell volume
RMSE	Root mean square of error
RSS	Residue sum of squares
SSA	Sobol sensitivity analysis
SV	Stroke volume
TPR	Total peripheral resistance
UO	Urine output
VR	Venous-return

Chapter 1: Introduction

1.1 Fluid Resuscitation

Intravenous fluid regulation has become a regular part of circulatory resuscitation in healthcare in decades since it keeps circulatory system within normal state while patients suffering from hypovolemia caused by trauma or infection. In today's clinical practice, most fluid resuscitation works are conducted by medical personnel or caretakers in a titration way. This continuous and heavy-workload task reveals some limitation and challenges and causes the desire of the autonomous systems in fluid resuscitation based on some reasons. First, the autonomous systems can optimize amounts of titration by acquiring information from different target end-points of patients, such as blood pressure, heart rate or urine output. With the optimal titration rate, the error and failure of the fluid regulation therapy can be reduced and stabilized. Second, autonomous infusion has better robustness than caretakers because it can deal with variabilities in physiological responses across different patients and different stages of trauma. Third, by maintaining long-term therapy with less error adjustments, the implementation of autonomous resuscitation systems can efficiently alleviate the workload of medical personnel and reduce the cost in medical treatments.

1.2 Autonomous Resuscitation System

Although autonomous closed-loop resuscitation systems have been studied for years, however, existing works in terms of controller design or model evaluation are still limited. Most closed-loop fluid resuscitation controllers in recent study are

designed and evaluated based on the naive decision-tree rules or simple controller gain tuning [1-4], which is lack of robustness and requires model-based design and approaches in the control-theory aspect to improve the autonomous resuscitation systems [5-9]. Besides, most autonomous resuscitation systems are evaluated by results of large-scale animal experiments [10-12], which are costly and time-consuming. Thus, for the time- and cost- efficient computation purpose, a credible system-level mathematical model that can efficiently capture the key phenomenon in circulation system and reproduce hemodynamic response to infusion or perturbation in non-clinical testing is beneficial to the field of evaluation and design autonomous resuscitation controller.

However, existing mathematical models for the purpose of reproducing hemodynamic response to perturbation of blood volume still have some limitations and do not fulfilled requirements discussed above. One class of existing black-box models can allow multiple infusions of various fluids to be specified and includes an estimation of the volumes, but they are too empiric to offer viable physical implications for clinical using [13-16]. Another class of existing models is first-principle model that comprehends all physiological phenomenon in human body. Because this kind of model involves hundreds parameters, it is too complex for computation and the purpose of closed-loop controller design [17-22]. Therefore, in order to address these challenges and limitations, the priority for the development of next generation closed-loop fluid resuscitation controller is constructing a simple and accurate mathematical model that suits for controller design and evaluation. For example, a model is able to reproduce hemodynamic responses, such as blood volume (BV), stroke volume (SV), cardiac

output (CO) and mean arterial pressure (MAP), to blood volume perturbation can be used as clinical endpoints in today's fluid resuscitation practice.

1.3 Thesis Goals and Outline

This thesis presents a lumped-parameter model to reproduce hemodynamic response to hemorrhage and fluid infusion that is able to apply to closed-loop fluid resuscitation controller evaluation. This model consist three different sub-models in different stages, including BV, CO and MAP sub-models, which are established in the fields of control theory and physiology, or developed base on our prior works [23]. Compare to existing hemodynamic models, the proposed model is unique based on two key characteristics. One of the characteristics is its simplicity, which only involves eleven parameters and is beneficial for establishing system-level feedback control action in autonomous systems. The other characteristic is its physiological transparency, which can be easily understood with control-mechanism system instead of using established physiological knowledge. In addition, the proposed model was examined by using animal experimental data collected from eleven sheep for its validity.

The thesis is organized as follows. In Chapter 2, a fully individualized hemodynamic model with three sub-models was studied and developed. In Chapter 3, we will apply this mathematical model to an experimental dataset collected from eleven sheep and perform system identification and sensitivity analysis and pick up some population-average candidate model for the further controller testing. In Chapter 4, we will apply the same control scheme using in the same animal experiment to the hemodynamic model and evaluate its validity through in-silico testing. In Chapter 5,

the thesis concludes with summary and outlining future work of this study.

Chapter 2: Model to Reproduce Hemodynamic Responses

2.1 Overview

As shown in Figure 2.1, The structure of the hemodynamic model in this thesis consists three sub-models which are able to reproduce three different responses individually, including (a) a control-theoretic blood volume (BV) model related to the perturbation such as fluid infusion or hemorrhage; (b) a physiologic-based cardiac output (CO) model to the perturbation of BV; (c) a control-theoretic mean arterial pressure (MAP) model related to the perturbation of CO.

In this chapter, we will introduce the structure of these three different sub-models, (a-c), in the hemodynamic model separately. After the structure of these three sub-models are well established, then we will also present how we combine them and develop the new hemodynamic model base on the knowledge these three sub-models.

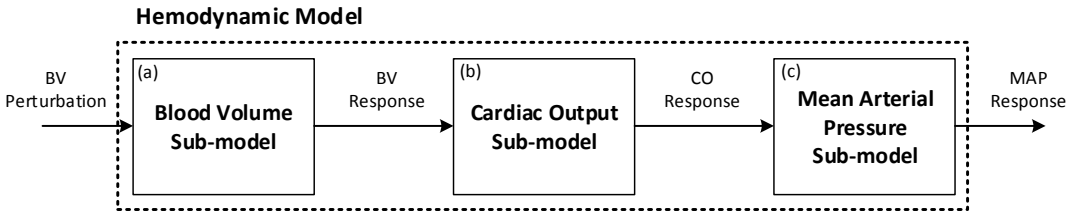

Fig. 2.1. The basic structure of hemodynamic model.

2.2 Three Sub-models

2.2.1 Modeling of Blood Volume Response to Blood Volume Perturbation

From the study in physiology, there are two major compartments contain the fluid in the human body, which are extracellular fluid (including plasma and interstitial fluid) and intracellular fluid (fluid contained in cells) [24]. In the observation of clinical practice, large-scale blood volume perturbation such as fluid infusion or hemorrhage occurs primary variation of fluid volume in the intravascular (plasma) compartment and interstitial fluid (ISF) compartment. However, due to the extracellular compartment is able to dynamically distribute fluid in plasma and ISF compartments via inter-compartmental shift, the fluid contained in two compartments can be regulated within specific range of ratio [24]. In our previous work, a model of BV response base on the feedback control theory and the knowledge of inter-compartmental fluid shift was developed [23]. The feedback control mechanism in this model was established base on the physiological principles of fluid distribution, which indicates that the volumetric change in the intravascular compartment is distributed to the plasma and the ISF with a certain ratio [24]. Based on this principle, the abstracting and complex inter-compartmental shift phenomenon can be simplified as a feedback control system with a simple compensator.

The fluid distribution ratio mentioned above varies depending on the physiological state of subject, which is determined by the vessel permeability, and hydraulic and osmotic pressure gradients at the capillary wall. However, from macroscopic standpoint, the consequence of the interaction among these complex

mechanisms is that the ratio between the volume changes in plasma and ISF can be summarized by a simple parameter value, denote here as α. Typically, ISF volume changes 2-3 times as much as plasma volume changes (i.e., α = 2-3). As shown in Figure 2.2, if blood volume is in the normal condition and does not beyond the critical blood volume, the relationship between the volumetric change of plasma and ISF can be consider as linear, which also means that α can be consider as a constant value. However, due to the composition in the fluids involved in infusion and hemorrhage processes are different (while the blood lost consists of plasma and red blood cells, the fluid infusion consist of crystalloid, such as Lactated Ringer's solution, or colloid, such as Hextend), the fluid distribution ratio in the steady state in response to fluid gain (fluid infusion) and fluid loss (hemorrhage and urine) are defined separately as two different constant value, which denote here as α_u (gain) and α_v (loss) respectively. Based on the principle of fluid shift, the desire steady-state change in plasma compartment, $r_{BV}(t)$, can be written as follows:

$$r_{BV}(t) = \frac{1}{1+\alpha_u}\int_0^t u(\tau)d\tau - \frac{1}{1+\alpha_v}\int_0^t v(\tau)d\tau \quad (2.1)$$

where u is the fluid infusion rate and v are the fluid loss rate, including hemorrhage and urine. With the value $r_{BV}(t)$ calculated from the Equation (2.1), the rate of inter-compartmental fluid shift (from plasma to ISF), $q(t)$, between the two compartments is determined by the discrepancy, $e_{BV}(t)$, between desire steady-state value, $r_{BV}(t)$, and actual BV volumetric change (plasma), ΔV_B, and can be written as follows:

$$q(t) = q(e_{BV}(t)) = q(r_{BV}(t) - \Delta V_B(t)) \quad (2.2)$$

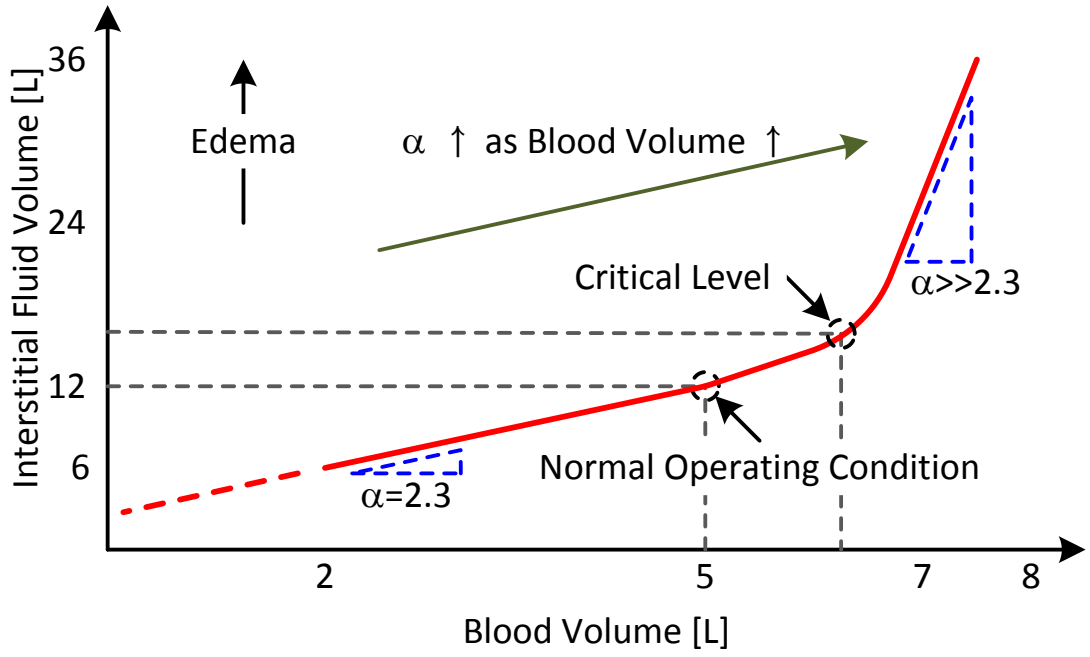

Fig. 2.2. Relationship between blood volume and interstitial fluid volume.

After the rate of fluid shift is calculated and apply to the intravascular compartment, the rate of change in ΔV_B at time t can be determined due to the conservation of fluid volume, which is equal to the summation of fluid gain ($u(t)$), fluid loss ($v(t)$), and outflow fluid shift ($q(t)$):

$$\Delta \dot{V}_B(t) = u(t) - v(t) - q(t) \tag{2.3}$$

For the fluid shift ($q(t)$), there is a simple proportional (P) controller control the rate and the direction (inflow or outflow) of the fluid shift, which strives the error between desired value and actual value of blood volume close to zero in steady state. Thus, the shift value in Equation (2.2) can be derived as follows:

$$q(t) = -K_p(r_{BV}(t) - \Delta V_B(t)) \tag{2.4}$$

where K_p is the proportional gain of the fluid shift controller, and the negative sign before K_p represents the outflow direction in intravascular compartment. By combining the Equation (2.1) – (2.4), the governing equation of fluid shift dynamics

can be written as follows:

$$\Delta\ddot{V}_B(t) + K_p\Delta\dot{V}_B = [\dot{u}(t) - \dot{v}(t)] + \frac{K_p}{1+\alpha_u}u(t) - \frac{K_p}{1+\alpha_v}v(t) \qquad (2.5)$$

As shown in Figure2.3, the structure of the BV sub-model can be visualized as a two-tank system connected with a fluid flow valve, where the two tanks represent plasma compartment and ISF compartment, and the valve represent the control mechanism of fluid shift.

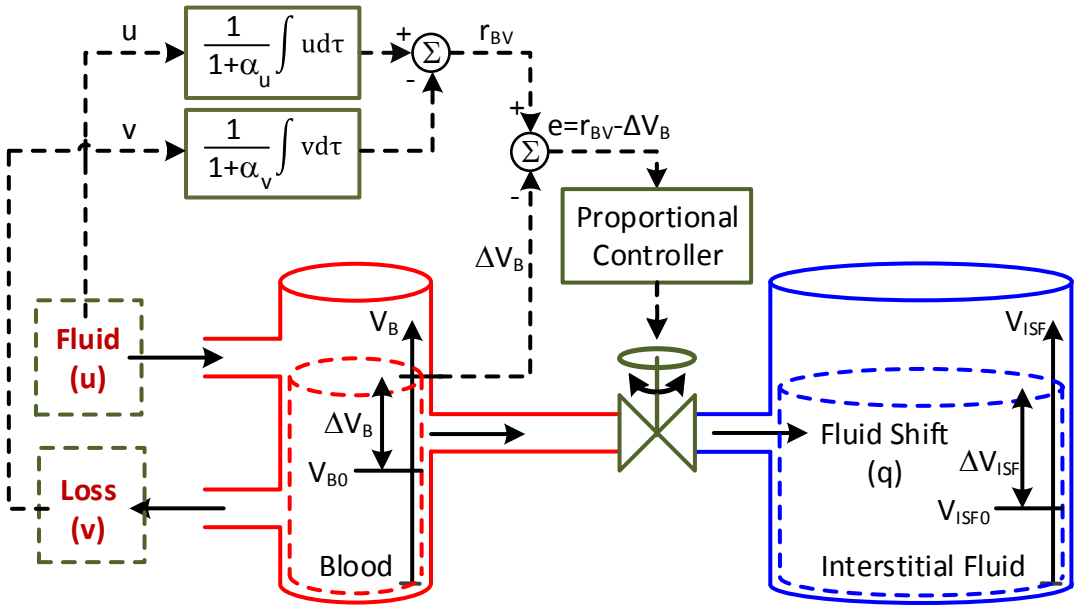

Fig. 2.3. A sketch of the blood volume sub-model.

2.2.2 Modeling of Cardiac Output Response to Blood Volume Changes

Because of the blood volume in intravascular compartment change, the cardiac output is also changed consequently at the vascular and ventricular standpoints. From the Arthur Guyton's previous work, he and his coworkers proposed a theory about venous-return (VR) system based on observations that as cardiac output (CO), which rate is similar to VR in steady state, was experimentally increased the right atrial

pressure decreased. The results illustrated that a volumetric perturbation in blood volume (BV) occurs variations in CO and VR, and their rate can be altered by the difference between mean systemic pressure (MSP) and central venous pressure (CVP) as follows [25]:

$$VR(t) = CO(t) = \frac{P_{MS}(t) - P_{CV}(t)}{R_{VR}} = \frac{P_{MS}(t) - P_{CV}(t)}{k \cdot TPR(t)} \tag{2.6}$$

where $P_{MS}(t)$ is MSP, $P_{CV}(t)$ is CVP, and R_{VR} is a hypothetical resistance to VR, which value is related to the elasticity and the muscle tissue of the venous return vessels, and it is proportional to the total peripheral resistance (TPR) in circulation system, $R_{VR} = k \cdot TPR(t)$. Besides, from the knowledge of MSP [25,26], the MSP can also be written as:

$$P_{MS}(t) = \frac{V_B(t) - V_{BU}}{C_s} = \frac{V_B(t) - \eta V_{B0}}{C_s} \tag{2.7}$$

where V_{BU} is unstressed BV, which is proportional to the normal state value or initial value of BV (before applying infusion or hemorrhage profile), and it denotes as the product of η and V_{B0}. C_s is also a hypothetical term that represents the systemic capacitance in circulation system [26]. By applying the Equation (2.7) to the Equation (2.6), the relationship of BV, CO, heart rate (HR) and stroke volume (SV) can be written as follows:

$$CO(t) = SV(t) \cdot HR(t) = \frac{1}{R_{VR}}\left[\frac{V_B(t) - \eta V_{B0}}{C_s} - P_{CV}(t)\right]$$

$$= \frac{1}{k \cdot TPR(t) \cdot C_s} V_B(t) - \frac{1}{k \cdot TPR(t)} P_{CV}(t) - \frac{\eta V_{B0}}{k \cdot TPR(t) \cdot C_s} \tag{2.8}$$

Furthermore, with the Frank-Starling Mechanism and the left ventricular (LV) pressure-volume loop relationship [27], the perturbation in SV and CO is occurred by the alteration in LV, which can be written as:

$$SV(t) = \frac{E_s}{E_s+E_A}(V_{ed}(t) - V_{B0}) = \frac{E_s}{E_s+HR(t)\cdot TPR(t)}(V_{ed}(t) - V_{B0}) \quad (2.9)$$

where $V_{ed}(t)$ is LV end diastolic volume (LVEDV), E_s is the LV elastance, E_A is the arterial elastance, which is also defined as the product of HR and TPR. By using the LV pressure-volume loop relationship and assuming blood volume in LV can represent the blood volume at the end of diastole state, the relationship between LVEDV, $V_{ed}(t)$, LV end diastolic pressure (LVEDP),$P_{ed}(t)$, can be written as:

$$V_{ed}(t) - V_{B0} = \frac{1}{A}\log(\frac{1}{B}P_{ed}(t) + 1) \quad (2.10)$$

where A and B are the constant parameters that define the shape of the LV pressure-volume loop [28,29]. Besides, The relationship between the $P_{CV}(t)$ in the Equation (2.8) and the $P_{ed}(t)$ in the Equation (2.10) is proportional, which we can assume $P_{ed}(t) \approx \gamma P_{CV}(t)$ [30] and combine the Equation (2.9) and the Equation (2.10) to the follows:

$$SV(t) = \frac{E_s}{E_s+HR(t)\cdot TPR(t)}\frac{1}{A}\log(\frac{\gamma}{B}P_{CV}(t) + 1) \quad (2.11)$$

Then, by combining the Equation (2.8) and the Equation (2.11), the direct relationship between $V_B(t)$ and $SV(t)$ can be obtained as following:

$$SV(t) = \frac{1}{A+\frac{A}{E_S}HR(t)\cdot TPR(t)}\log(-\frac{\gamma k}{B}TPR(t)\cdot CO(t) + \frac{\gamma}{BC_s}V_B(t) - \frac{\gamma}{BC_s}\eta V_{B0} + 1)$$

(2.12)

By multiplying the heart rate, $HR(t)$, to the Equation (2.12), the direct relationship between $V_B(t)$ and $CO(t)$ yields as follows:

$$CO(t) = HR(t)\cdot\frac{1}{\theta_1+\theta_2 HR(t)\cdot TPR(t)}\log(\theta_3 TPR(t)\cdot CO(t) + \theta_4 V_B(t) - \theta_4\theta_5 V_{B0} + 1)$$

(2.13)

where $\theta_1 = A$, $\theta_2 = \frac{A}{E_s}$, $\theta_3 = -\frac{\gamma k}{B}$, $\theta_4 = \frac{\gamma}{BC_s}$, and $\theta_5 = \eta$. These parameters are the only five constant parameters that need to be tuned individually to the measurement data of each specific subject. As shown in Figure 2.4, the structure of the CO sub-model can be visualized as a combination of LV pressure-volume loop relationship (Equation (2.11)) and VR system (Equation (2.6)). With the development of CO sub-model, the CO can be reproduced responses due to the BV change can be derived from the Equation (2.13).

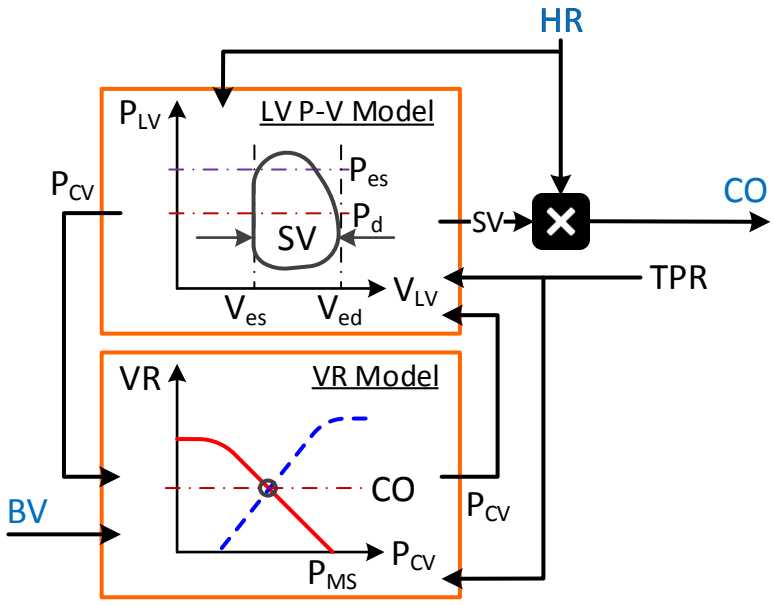

Fig. 2.4. A sketch of the cardiac output sub-model.

2.2.3 Modeling of Mean Arterial Pressure Response to Cardiac Output Changes

Due to the cardiac output (CO) in the blood circulation system change, the mean arterial pressure (MAP) is also varied consequently. In Guyton's previous work, the blood circulation system is able to regulate the blood pressure within some specific constant levels even patients experience hemorrhage, which variations of MAP can be compensated by increasing or decreasing the total peripheral resistance (TPR) via the

arterial autonomic-cardiac regulation [31,32]. Although the first principles nature of physiology mechanism are complex, the mechanism of the arterial autonomic-cardiac regulation can abstract into a feedback control system based on the observation of animal experimental dataset and the knowledge from previous study related to baroreflex mechanism.

From the observation of the MAP dataset of 11 sheep, we found consistently in all the subjects that the arterial autonomic-cardiac regulation system brought the MAP back to the normal steady level in the end even the subjects experience a hemorrhage and their CO and BP decrease with a tremendous amount in the beginning stage. This phenomenon of physiological reaction is quite similar to the results from the studies of baroreflex system [33-35], which provides a rapid negative feedback loop in which an elevated blood pressure reflexively causes the heart rate to decrease and also causes blood pressure to decrease. Besides, since the CO sub-model in the Section 2.2.2 incorporates the feedback information of TPR to update the CO sub-model, the MAP sub-model also requires the ability to implement the change of TPR and feedback the TPR information to the CO sub-model. Thus, by borrowing the idea from baroreflex system and the goal of reproducing TPR response, a TRR and MAP control-theoretic sub-model was established as shown in Figure 2.5. In this sub-model, the compensator can tune the change of TPR, $\Delta TPR(t)$, due to the difference, $e(t)$, between of the MAP target value and actual value, which relationship can be written as following:

$$\Delta TPR(t) = f\big(e(t)\big) = f\big(MAP_{target} - MAP(t)\big) \tag{2.14}$$

where f is the transfer function of compensator that defines the relationship between the $e(t)$ and $\Delta TPR(t)$, and MAP_{target} is a hypothetical constant parameter that

represents the desired value of MAP which the compensator aims to track and follow. For the first approach in this study, the nominal value of this target value of MAP was assumed to be the average of the steady-state MAP value (in the last half hour) of the animal experimental dataset. Furthermore, the value of MAP at time t instant can be consider as the product of CO and TPR, which relationship between these three terms can be written as follows:

$$MAP(t) = CO(t) \cdot TPR(t) = CO(t) \cdot [TPR_0 + \Delta TPR(t)] \qquad (2.15)$$

where TPR_0 is the initial value of TPR, which is defined from initial value of CO and MAP, $TPR_0 = \frac{MAP_0}{CO_0}$. For an example that can be better understood, when a subject experiences a hemorrhage and its CO decreases consequently, the actual value of MAP will drop below to the target value of MAP in the block diagram based on the Equation (2.15). Then, the compensator calculates the change of TPR, $\Delta TPR(t)$, due to the difference between the target and actual MAP values in the Equation (2.14) (In this case, the $\Delta TPR(t)$ is positive due to the difference is positive). By increasing TPR, the decreasing of CO can be compensated to strive the MAP back to the desired value, MAP_{target}.

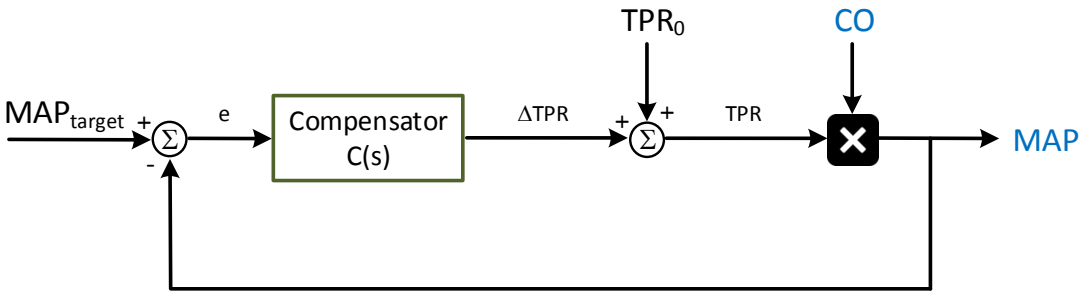

Fig. 2.5. A sketch of the mean arterial pressure sub-model.

In order to find the best compensator with less complexity and better performance

to represent the physiological mechanism in the real world, different type of compensators had been investigated and evaluated. J.T. Ottesen proposed a model for the human cardiovascular control system and illustrated two important parts of the automatic central nervous system for controlling the heart and the capillaries, which are the sympathetic (relatively slow-acting) and the vagal (relatively fast-acting) nervous systems as shown in Figure 2.6 [36,37]. There has also been other evidence presented that the sympathetic control of TPR (capillaries) has more contribution to the oscillation in blood pressure than the sympathetic feedback to the heart muscle or heart rate change [38,39,40]. Besides, the renin-angiotensin system also takes part in the human cardiovascular control system, which enable to vary the concentration of a peptide hormone, angiotensin, to regulate blood pressure [41]. Briefly speaking, the period of the cyclic oscillation in blood pressure due to the β-sympathetic signal, which control the TPR (capillaries) , is similar to the period of respiration at about 3-6 seconds, while the cyclic oscillation in blood pressure due to the renin-angiotensin system is a relatively slow-acting effect, which period of oscillation is at about hours. Since the dynamic of baroreceptors are much faster than these two control mechanisms, we also assumed that there is no transport delay in the feedback loop in the Figure 2.5.

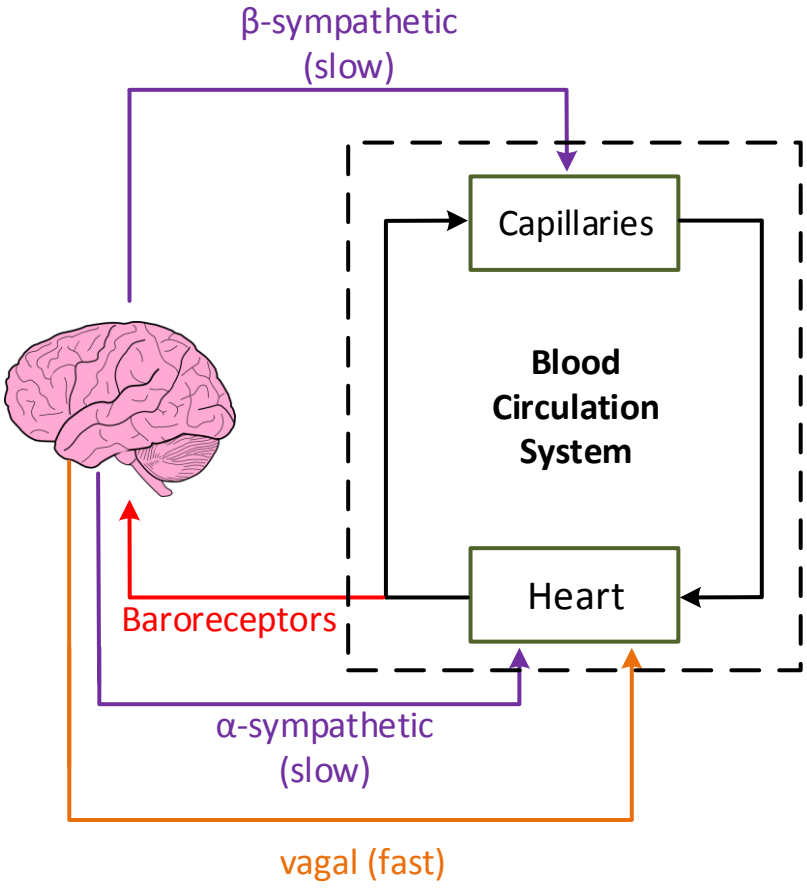

Fig. 2.6. A sketch of the baroreflex cardiac control system.

Consider the β-sympathetic nervous system as the short-term (fast) effect and the renin-angiotensin system as the long-term (slow) effect in the human cardiovascular control of TPR, we assume the transfer function, $C(s)$, of the forward loop compensator in the Figure 2.5 is $\frac{n_1(\cdot)}{s+p_1}+\frac{n_2(\cdot)}{s+p_2}$ (Type 1), where p_1 and p_2 represent the transient dynamic properties (related to time constant), and $n_1(\cdot)$ and $n_2(\cdot)$ represent the nonlinear gain (sigmoid curvature defined by a parameter) of the two systems, and the structure of this compensator is shown in the Figure 2.7 (a). However, because of the limitation of sparse animal experimental dataset (5 minutes time interval), the fast dynamic of β-sympathetic nervous system might not be observed in the identification results. Thus, we simplify the fast dynamic component as a simple

nonlinear gain, and the transfer function, $C(s)$, becomes $\frac{n_1(\cdot)}{s+p_1} + n_2(\cdot)$ (Type 2), which can be shown in the Figure 2.7 (b). Furthermore, after we analyze the identification results of MAP sub-model with Type 1 and Type 2 compensator by using the CO and MAP data of experimental measurement, we found that the nonlinear gain of fast dynamic is trivial in the both cases. As the result, we further simplify the compensator as $\frac{n_1(\cdot)}{s+p_1}$ (Type 3) as shown in the Figure 2.7 (c). Except for assuming the gains in compensator are nonlinear, the linear-gain cases had also been studied. We replaced the nonlinear gains in Type 2 and Type 3 compensator by linear gains, which the transfer function become $\frac{k_1}{s+p_1} + k_2$ (Type 4) and $\frac{k_1}{s+p_1}$ (Type 5) as shown in the Figure 2.7 (d) and (e).

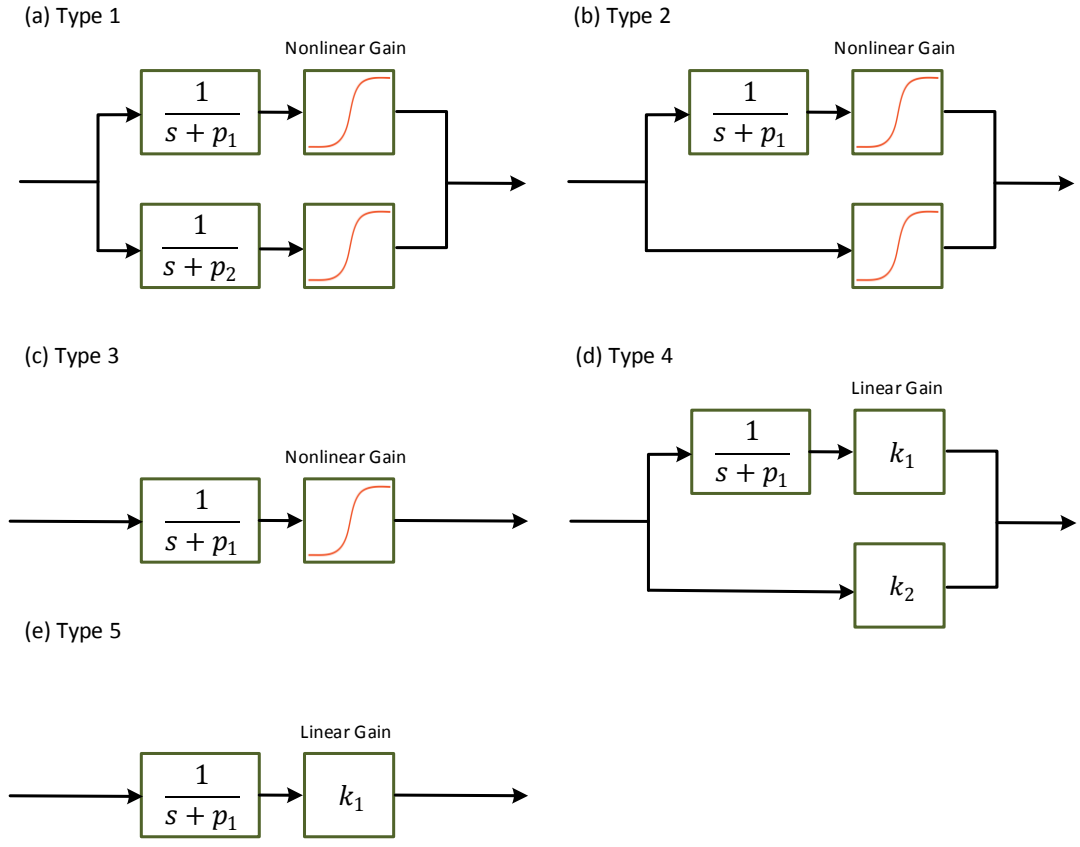

Fig. 2.7. A sketch of the different type compensators.

After applying these five compensator to the system identification of MAP sub-model, the fitting performances of each compensators can be quantified by calculating the residue sum of squares (RSS) of fitting MAP error among eleven subjects, which the equation of RSS is defined as follows:

$$RSS = \sum_{i=1}^{n}\left(MAP(t_i) - \widehat{MAP}(t_i)\right)^2 \tag{2.16}$$

where $MAP(t_i)$ and $\widehat{MAP}(t_i)$ are the measurement value and the model prediction of MAP at time t_i, n is the sample size of the MAP data. The fitting results of these five compensator are shown and compared in the Table 2.1. Besides, in order to analyze the accuracy-complexity trade-off between five compensators, the corrected Akaike information criterion (AICc) [42] of five compensators for each subjects are also calculated and compared subject-specifically, which value combines the fitting performance (RSS) and dimension of the model (number of identified parameters) and the equation is defined as follows:

$$AICc = n\log\left(\frac{RSS}{n}\right) + 2k + \frac{2k(k+1)}{n-k-1} \tag{2.17}$$

where k is the number of identified parameters in the sub-model and RSS is from the Equation (2.16). The AICc results of compensators are compared and shown in the Table 2.2.

RSS	Type 1	Type 2	Type 3	Type 4	Type 5
Number of Parameters	5	4	3	3	2
Avg. [mmHg]	36.91	36.76	37.02	37.07	37.11

Table 2.1. RSS of the predicted versus measured MAP

AICc	Type 1	Type 2	Type 3	Type 4	Type 5
Number of Parameters	5	4	3	3	2
Subject 1	2.42	0.38	-3.14*	16.27	13.98
Subject 2	30.45	26.86	24.11	23.80	21.37*
Subject 3	-13.31	-20.46	-18.81	-21.36	-21.42*
Subject 4	29.77	26.96	24.23	24.28	21.76*
Subject 5	14.87	13.48	10.18	12.08	9.18*
Subject 6	3.20	7.13	4.98	-1.11	-1.92*
Subject 7	11.44	6.03	-2.06	-4.85	-6.46*
Subject 8	16.51	15.39	12.84	1.54	-1.00*
Subject 9	18.51	15.66	13.02	12.95	10.43*
Subject 10	17.29	8.09	11.58	7.93	2.64*
Subject 11	11.10	8.17	5.41*	8.87	6.35

Table 2.2. AICc results of five compensators

As the RSS results in Table 2.1, we can find that even we increase the number of parameters (complexity) in compensator, the sum of the fitting errors RSS of eleven subjects are still similar, which means the fitting performance cannot be improved by increasing its complexity of the compensator. Thus, based on the AICc results in Table 2.2, we picked the simplest compensator, which is one-pole compensator with linear gain (Type 5), for the future study since it has less AICc in the 9 of 11 subjects. Besides,

by applying the transfer function of this compensator, $C(s) = \frac{k}{s+p}$, to the f in the Equation (2.14) and combining the Equation (2.15), the governing equation of the feedback control system of the MAP sub-model can be written as:

$$MAP(t) = CO(t) \cdot \left\{ TPR_0 + \mathcal{L}^{-1}\left[C(s) \cdot \left(\frac{MAP_{target}}{s} - MAP(s) \right) \right] \right\} \quad (2.18)$$

With computation in the Equation (2.18), the MAP sub-model can successfully reproduce MAP responses and TPR responses to CO perturbation.

2.3 Hemodynamic Model

After deriving bunch of equations in the previous section, three different sub-models are now well defined and have abilities to reproduce responses of different endpoints, such as blood volume (BV), stroke volume (SV), cardiac output (CO), total peripheral resistance (TPR) and mean arterial pressure (MAP). Besides, in each sub-model, the ports of input and outputs are related to each other, like the output in BV sub-model and input in CO sub-model are both $V_B(t)$, and the output in CO sub-model and one of the input in MAP sub-model are both $CO(t)$.

Thus, for the purpose that discuss in the Chapter 1.3, which is establishing a simple but sufficient lumped-parameter model that can reproduce hemodynamic response to blood volume perturbation for the future closed-loop resuscitation controller design and evaluation, we combined the Equation (2.5), (2.13) and (2.18) in the previous sections to develop a BV-CO-MAP hemodynamic model as shown in the Figure 2.8. Note that the total peripheral resistance (TPR) in part (c) of the Figure 2.8 feedbacks to the part (b) to update the TPR terms in the Equation (2.13). With this BV-

CO-MAP hemodynamic model, the responses of BV, SV, CO, TPR and MAP can be reproduced with given input profile, including infusion ($u(t)$), blood loss ($v(t)$), and heart rate ($HR(t)$).

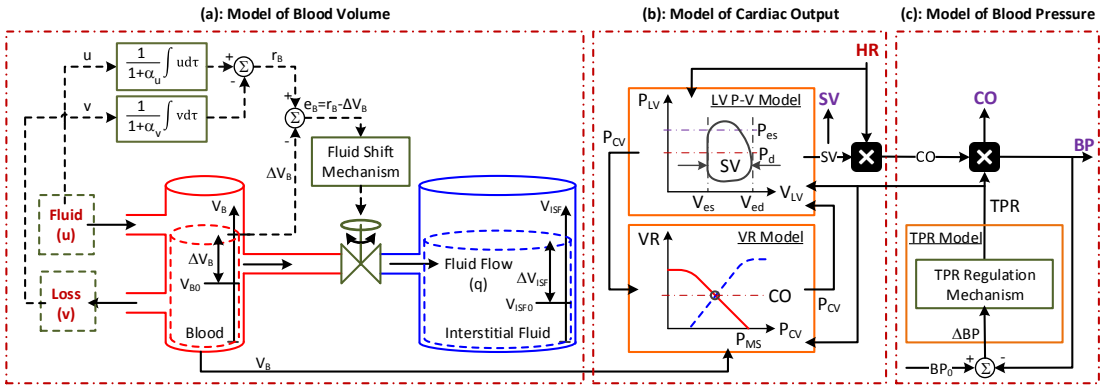

Fig. 2.8. A sketch of the BV-CO-MAP hemodynamic model

Chapter 3: System Identification and In-silico Evaluation

3.1 Overview

In the previous Chapter, we have presented a lumped-parameter model that can reproduce hemodynamic response of different endpoints to blood volume perturbation. In this chapter, we will further analyze and validate this model by fitting the model estimated blood volume (BV), cardiac output (CO), and mean arterial pressure (MAP) responses with the measurements collected from the eleven sheep which dataset comes from an animal experiment under the protocol approved by the Institutional Animal Care and Use Committee (IACUC) at the University of Texas Medical Branch, Galveston [10].

In order to see if the model is able to be adapted to different specific subjects, we will perform fully individualized model identification via numerical optimization (subject-specific evaluation) in the following section and compare the system identification results with a model from previous work to see if the adaptive ability of the new model has been improved. After analyzing the subject-specific identified model, we also applied the controllers used in the animal experiment [43], including decision-tree, PID, Fuzzy logic controllers, to the subject-specific identified model and did in-silico closed-loop control evaluation to see if the model can reproduce similar responses to the experiment in different endpoints. Furthermore, we also randomized the parameters in the model to examine the performance of these three types of controllers with different criterion.

3.2 Experimental Data

In the experiments, all 11 animals received Lactated Ringer's solution (LR) and 5 of them also receive Hex solution as fluid infusion. For the 5 animals which received both kinds of fluids, the experiments of each fluid infusion were conducted separately and at least 5 days apart. The duration of the experimental study for each subject was 3 hours. Based on the records of experiments, after the baseline data of subjects, such as blood volume and blood pressure in normal state, were recorded, the subject experienced an initial major hemorrhage, which quantity is determined based on the weight of subject (25ml/kg), lasting around 15 minutes. Then, fluid infusion was started 30 minutes after the start of the major hemorrhage and continued for the rest 150 minutes. Except for the major hemorrhage experienced in the beginning stage, there are also second and third relatively minor hemorrhages (both are 5ml/kg) were conducted 20 and 40 minutes after the start of the fluid infusion, and each hemorrhage lasted for 5 minutes.

For the fluid infusion profile, the control input profiles of 6 subjects were performed automatically based on a decision-tree rule-based closed-loop controller, which rules were described in previous publication [10,43-44]. In the details of this decision-tree rule, a maximum fluid infusion was set to be 100 ml/min per 70 kg when mean arterial pressure (MAP) measurement values of subjects was equal to or below 40 mmHg, 80% of the maximum fluid infusion rate was given to subjects when their MAP measurement values were between 41 and 44 mmHg, 60% of the maximum fluid infusion rate was given to subjects when their MAP measurement values were between 45 and 49 mmHg, 30% of the maximum fluid infusion rate was given to subjects when

their MAP measurement values were between 50 and 69 mmHg, and 10% of the maximum fluid infusion rate was given to subjects when their MAP measurement values were between 70 and 89 mmHg. For the case that the MAP measurement values of subjects were equal to or above 90 mmHg, there was no fluid infusion.

In each subject, baseline blood volume (BV) was measured by using indocyanine green dye (ICG) method [45]. Furthermore, the Hematocrit, which is defined as the ratio between the red blood cell volume (RBCV) and BV, of each subject was measured before and throughout the experiment with 5 minutes time-interval to measure the BV change at time instants. Other hemodynamic responses, including cardiac output (CO), heart rate (HR) and MAP, were also measured simultaneously at the same time instants.

3.3 System Identification

In this section, we will perform fully individualized model identification of the proposed BV-CO-MAP hemodynamic model to evaluate its ability and performance and determine if the model is well-conditioned. By fitting the hemodynamic responses of model to experimental data of subjects individually, we can investigate if the model is able to be adapted to the subjects and reproduce reasonable subject-specific responses of different endpoints. Besides, the fitting results of fully individualized models were also compared in terms of accuracy and accuracy-complexity trade-off with the other BV-CO-MAP model from our previous work (2017 version) [46].

3.3.1 Individualized Model Identification and Analysis

The fully individualized system identification of BV-CO-MAP hemodynamic model was performed by using numerical optimization method. This model consists

three sub-models, and there are tunable 11 constant parameters in total: 3 in the Equation (2.5) ($\alpha_u,\ \alpha_v,\ K_p$) of the BV sub-model; 5 in the Equation (2.13) ($\theta_1,\ \theta_2,\ \theta_3,\ \theta_4,\ \theta_5$) of the CO sub-model; and 3 in the Equation (2.18) ($k,\ p,\ MAP_{target}$) of the MAP sub-model. The upper bound, lower bound of these 11 constant parameters are defined based on the study of previous literature of physiology [23-41], which are listed in Table 3.1, where Avg is be the average of the steady-state MAP value (in the last half hour) of the animal experimental dataset.

Parameters	α_u	α_v	K_p	θ_1	θ_2	θ_3	θ_4	θ_5	k	p	MAP_{target}
Unit	[·]	[·]	[·]	$[ml^{-1}]$	[mmHg·min]	[mmHg]	$[ml^{-1}]$	[·]	[·]	[·]	[mmHg]
Upper Bound	6	6	0.5	0.3	0.001	0	0.1	1	1	1	Avg+20
Lower Bound	0	0	0.01	0	0	-0.001	0	0.2	0	0	Avg-20

Table 3.1. Upper and lower bounds of the identified parameters in model

After the optimization setting discussed above was defined, we give input profiles (including fluid infusion, hemorrhage, urine output and heart rate measurement data), fitting reference (including BV, CO, and MAP experimental measurement data) and a set of initial parameter estimates (starting point of optimization) to optimization problems setting and minimize the fitting error. More specifically, the optimization problems were solved via the optimization tools available in MATLAB Optimization Toolbox [47] to minimize the discrepancy between model prediction and actual

measurements defined as following:

$$\theta^* = \{\alpha_u, \alpha_v, K_p, \theta_1, \theta_2, \theta_3, \theta_4, \theta_5, k, p, MAP_{target}\}$$
$$= arg\min_{\theta} \left(\left\| \frac{\widehat{V_B}(t) - V_B(t|\theta)}{\overline{\widehat{V_B}(t)}} \right\|_2 + \left\| \frac{\widehat{CO}(t) - CO(t|\theta)}{\overline{\widehat{CO}(t)}} \right\|_2 + \left\| \frac{\widehat{MAP}(t) - MAP(t|\theta)}{\overline{\widehat{MAP}(t)}} \right\|_2 \right) \quad (3.1)$$

where θ^* is optimum value of θ minimize the cost function in the Equation (3.1), $\widehat{V_B}(t)$, $\widehat{CO}(t)$, and $\widehat{MAP}(t)$ are BV, CO, and MAP experimental measurement data, while $V_B(t|\theta)$, $CO(t|\theta)$, and $MAP(t|\theta)$ are the predicted BV, CO, and MAP response of the model with optimized parameters θ^*, which simulation time step of t is as same as the intervals using in the dataset. $\overline{\widehat{V_B}(t)}$, $\overline{\widehat{CO}(t)}$, and $\overline{\widehat{MAP}(t)}$ are the averages of each variable over the entire experiment. With these three averages, the error magnitudes in BV, CO, and MAP components can be normalized to the same scale.

The optimization problem (3.1) was solved via pure (infinite-step-ahead) prediction. One of the fitting results, including input profile, BV, SV, CO, TPR and MAP fitting, of crystalloid cases (LR) are shown in Figure 3.1, and one of the fitting results of colloid cases (Hex) are shown in Figure 3.2. Table 3.2 shows the RMSEs associated with the BV-CO-MAP hemodynamic models in reproducing BV, CO, and MAP (mean (SD)). Table 3.3 shows the corresponding optimized parameters and their mean (SD).

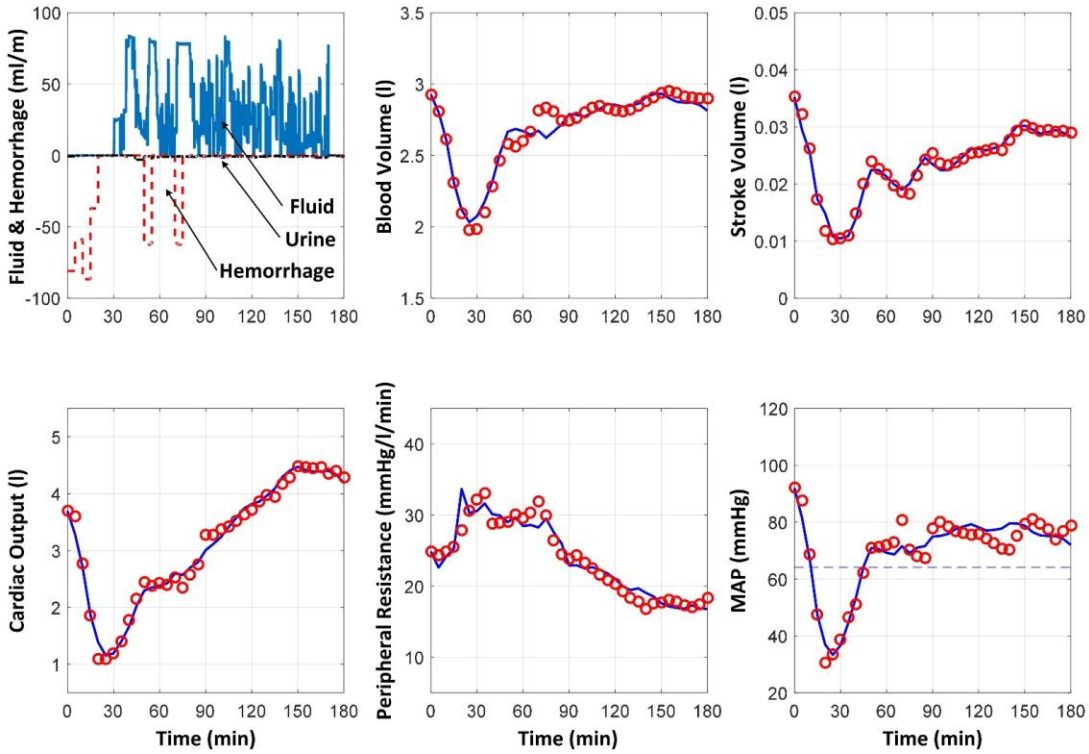

Fig. 3.1. Measured versus model-predicted response to crystalloid infusion case

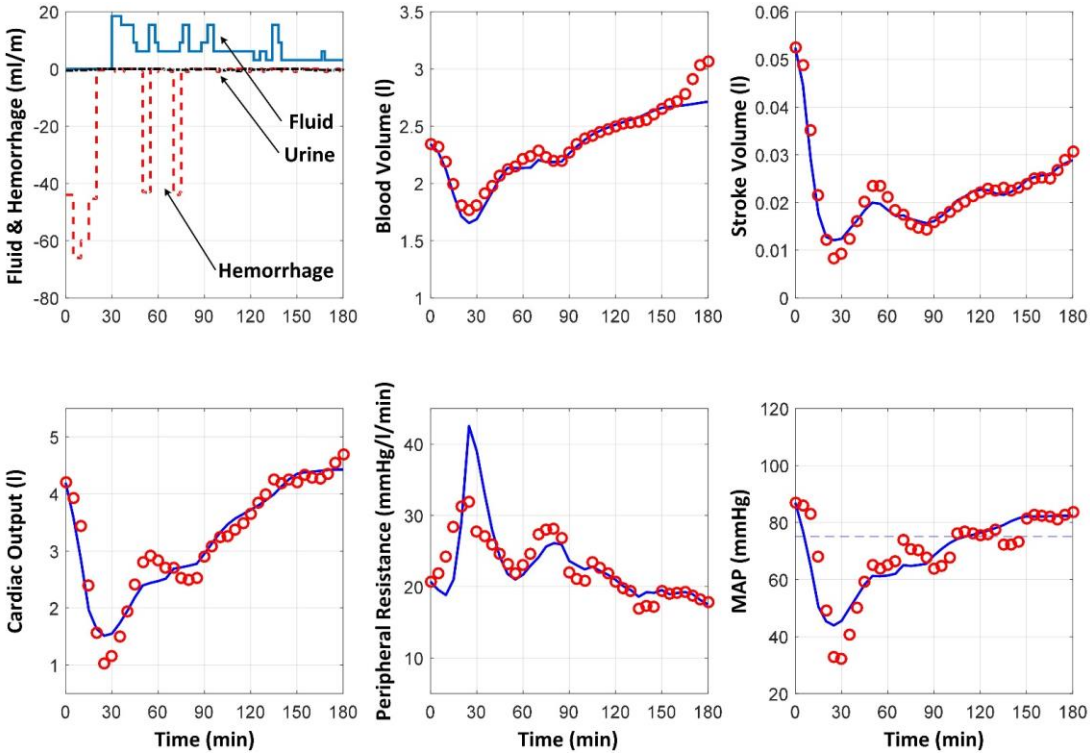

Fig. 3.2. Measured versus model-predicted response to colloid infusion case

(a) Crystalloid

Subject	BV error [l]	CO error [lpm]	MAP error [mmHg]
1	0.09	0.19	4.75
2	0.08	0.33	7.88
3	0.08	0.17	3.54
4	0.11	0.38	7.86
5	0.11	0.42	6.20
6	0.08	0.36	7.37
7	0.04	0.17	4.46
8	0.07	0.12	3.97
9	0.19	0.27	8.83
10	0.11	0.19	5.15
11	0.07	0.19	7.11
Mean (SD)	0.09 (0.04)	0.25 (0.10)	6.10 (1.81)

(b) Colloid

3	0.16	0.18	3.79
4	0.06	0.12	5.97
5	0.06	0.30	6.14
6	0.10	0.24	6.60
7	0.07	0.20	7.86
Mean (SD)	0.09 (0.04)	0.21 (0.07)	6.07 (1.47)

Table 3.2. RMSEs associated with the individualized models

(a) Crystalloid

Subject	α_u	α_v	K_p	θ_1	θ_2	θ_3	θ_4	θ_5	k	p	MAP_{target}
1	1.17	0.98	0.14	0.21	4.54e-5	-3.09e-5	0.01	0.65	0.01	0.00	91.40
2	1.78	0.30	0.07	0.29	9.41e-5	-5.45e-6	0.02	0.41	0.02	0.06	68.45
3	5.77	5.55	0.08	0.27	3.56e-5	-2.87e-6	0.01	0.21	0.54	0.67	82.01
4	1.30	0.54	0.04	0.24	4.82e-4	-9.25e-10	0.10	0.46	0.01	0.02	81.11
5	5.94	0.69	0.03	0.05	9.29e-5	-8.34e-5	0.01	0.40	0.45	0.71	61.69
6	3.50	2.03	0.08	0.08	1.50e-4	-3.17e-7	0.01	0.31	0.01	0.00	62.36
7	5.37	4.68	0.08	0.24	4.73e-4	-3.70e-8	0.04	0.49	0.16	0.38	62.89
8	5.58	1.20	0.07	0.17	1.02e-4	-2.14e-6	0.01	0.49	0.01	0.02	64.11
9	1.12	0.75	0.07	0.11	1.09e-5	-5.98e-10	0.00	0.42	0.05	0.02	69.06
10	2.28	0.53	0.03	0.26	3.01e-5	-2.15e-5	0.01	0.41	0.16	0.73	109.24
11	2.34	1.47	0.12	0.07	1.23e-4	-9.43e-5	0.02	0.48	0.32	0.62	83.49
Mean (SD)	3.29 (2.00)	1.70 (1.77)	0.07 (0.03)	0.18 (0.09)	1.49e-4 (1.98e4)	-2.19e-5 (3.47e-5)	0.02 (0.03)	0.43 (0.11)	0.16 (0.19)	0.29 (0.33)	75.98 (15.07)

(b) Colloid

3	-0.03	1.70	0.17	0.24	2.76e-4	-5.31e-5	0.02	0.23	0.40	0.59	83.21
4	0.13	1.15	0.08	0.04	4.90e-5	-6.18e-5	0.02	0.63	0.02	0.05	77.04
5	1.36	5.97	0.05	0.15	2.89e-4	-1.15e-6	0.02	0.38	0.02	0.10	66.35
6	0.39	2.67	0.06	0.23	4.57e-4	-3.87e-7	0.02	0.22	0.06	0.22	75.11
7	0.43	2.66	0.03	0.29	5.87e-4	-6.01e-10	0.03	0.25	0.12	0.33	55.00
Mean (SD)	0.46 (0.54)	2.83 (1.87)	0.08 (0.06)	0.19 (0.10)	3.32e-4 (2.04e-4)	-2.33e-5 (3.13e-5)	0.02 (0.01)	0.34 (0.17)	0.12 (0.16)	0.26 (0.21)	71.34 (10.95)

Table 3.3. List of corresponding optimized parameters

3.3.2 Comparison with a Hemodynamic Model from Previous Work

From our previous work [47], a similar BV-CO-MAP hemodynamic model was developed in 2017. The major discrepancies between the previous model and the model in this thesis are the structure of the MAP sub-model and the feedback action of total peripheral resistance (TPR) between the CO sub-model and the MAP sub-model. In the structure of MAP sub-model, while the new version was developed based on the feedback control theory that we mentioned in the Section 2.2.3, the previous version of MAP sub-model was established based on the autonomic-cardiac regulation phenomenon and a sigmoidal relationship between TPR and MAP [31,32]. On the other hand, the new version of the hemodynamic model is able to feedback and update the TPR term in the CO sub-model, while the previous version of CO sub-model is similar to the Equation (2.13) but keep TPR as a constant value without updating.

The identification fitting results of two different models were compared as shown in Table 3.4, which listed the normalized BV, CO and MAP fitting error of two different models in both fluid (unit and percentage). As the results in Table 3.4, the new version BV-CO-MAP model has remarkable improvements in the CO fitting and MAP fitting.

(a) Crystalloid

	BV error [l] (%)	CO error [lpm] (%)	MAP error [mmHg] (%)
Model 2017	0.10 ± 0.04 (5 ± 2%)	0.48 ± 0.21 (13 ± 4%)	8.97 ± 2.31 (12 ± 3%)
Model 2018	0.09 ± 0.04 (4 ± 2%)	0.25 ± 0.10 (7 ± 2%)	6.10 ± 1.81 (8 ± 2%)

(b) Colloid

	BV error [l] (%)	CO error [lpm] (%)	MAP error [mmHg] (%)
Model 2017	0.06 ± 0.02 (3 ± 1%)	0.39 ± 0.14 (13 ± 4%)	8.04 ± 3.77 (12 ± 5%)
Model 2018	0.09 ± 0.04 (4 ± 2%)	0.21 ± 0.07 (6 ± 1%)	6.07 ± 1.47 (8 ± 3%)

Table 3.4. RMSEs of previous model versus recent model

3.4 In-silico Closed-loop Control Evaluation

After the identification results shows that the model is well-conditioned and enable to adapt to different subject in real world, we also apply the controller, which are identical to the ones used in experiments, to the identified model to see if the closed-loop control system can reproduce the similar results. Besides, the performance of the controller, including decision-tree, PID and fuzzy logic controller, was examined by randomly perturb the parameters in the model and see if the controller can deal with the variation.

3.4.1 Closed-loop Feedback Controllers

Based on the closed-loop system description in the experiment [43], 6 of 11 subjects were applied to the decision-tree controllers, 4 of 11 subjects were applied to the PID controllers and 1 of 11 subjects was applied to fuzzy logic controller.

In order to make the decision-tree controllers be able to reach and maintain MAP at a desired level, the table of decision algorithm was defined as: (a) a maximum fluid infusion was set to be 100 ml/min per 70 kg when mean arterial pressure (MAP)

measurement values of subjects was equal to or below 40 mmHg, (b) 80% of the maximum fluid infusion rate was given to subjects when their MAP measurement values were between 41 and 44 mmHg, (c) 60% of the maximum fluid infusion rate was given to subjects when their MAP measurement values were between 45 and 49 mmHg, (d) 30% of the maximum fluid infusion rate was given to subjects when their MAP measurement values were between 50 and 69 mmHg, (e) and 10% of the maximum fluid infusion rate was given to subjects when their MAP measurement values were between 70 and 89 mmHg. (f) For the case that the MAP measurement values of subjects were equal to or above 90 mmHg, there was no fluid infusion.

For the proportional-integral-derivative (PID) controllers, the gains of the proportional, integral, and derivative terms are 0.025, 0.07, and 0.05. For the algorithm of fuzzy logic controller, it uses two linear input fuzzy sets for each of two input signals, which are MAP error and rate change of MAP error, four Takagi-Sugeno fuzzy control rules with the simplified linear rule consequents, and the centroid defuzzifier. This fuzzy logic controller can be considered as a nonlinear proportional-integral (PI) with variable gains. By changing the gains based on the two input signals, the performance of controller can be improved compare with the linear controllers, especially for the nonlinear systems.

3.4.2 In-silico Closed-loop Control Systems Evaluation

Except for analyzing open-loop system in the Section 3.3, which excludes the controller component and only uses input-output data, the closed loop control system was also evaluated by applying these 3 different types of controllers to the each identified model subject-specifically. The Figure 3.3 shows the measured versus model-

predicted responses of closed-loop control system, and the Table 3.5 lists the normalized RMSEs (NRMSE) of two responses in different controller cases.

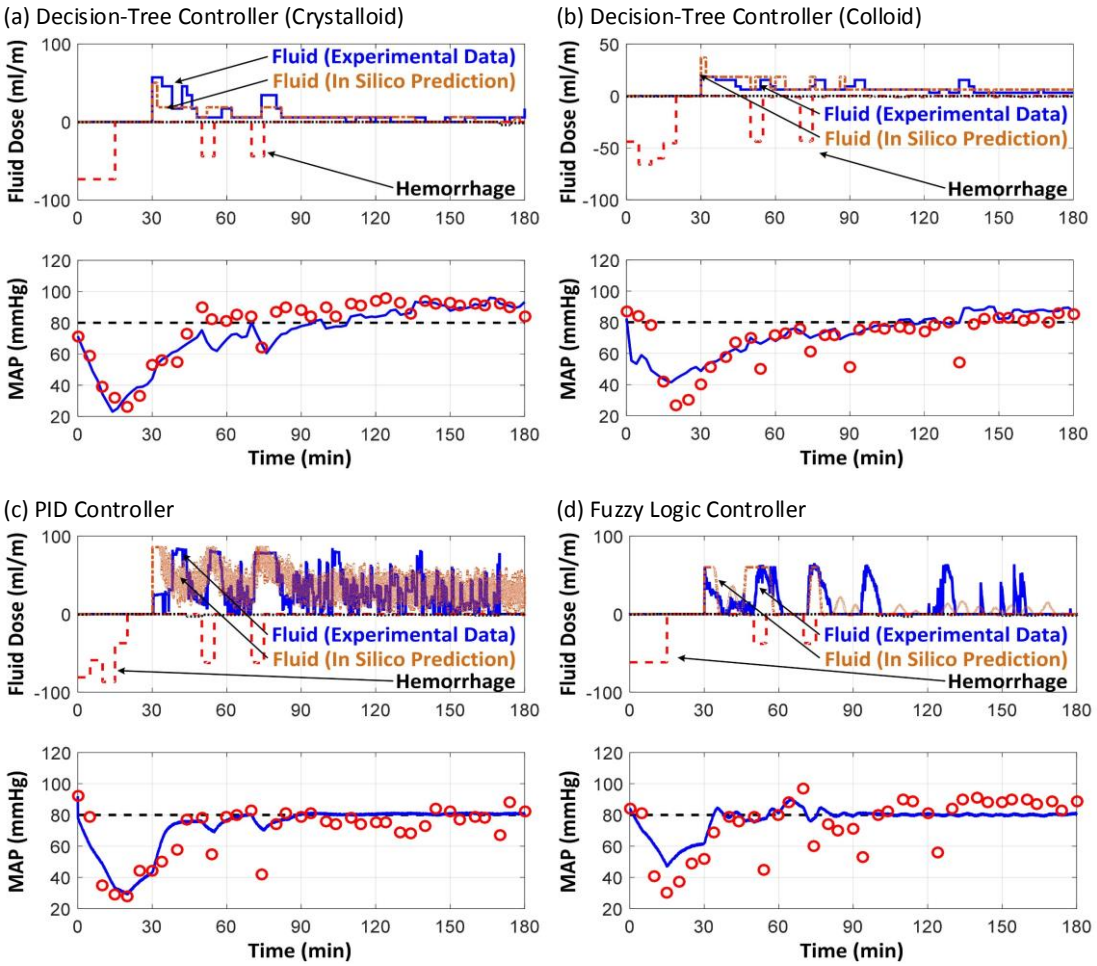

Fig. 3.3. Measured versus model-predicted responses of closed-loop control system

NRMSE	N	BV [l] (%)	CO [lpm] (%)	MAP [mmHg] (%)
DT (Crystalloid)	6	0.14 ± 0.08 (6 ± 2%)	0.79 ± 0.40 (21 ± 10%)	7.15 ± 2.47 (10 ± 3%)
DT (Colloid)	5	0.15 ± 0.12 (7 ± 6%)	0.53 ± 0.22 (16 ± 6%)	7.32 ± 1.69 (10 ± 3%)
PID	4	0.14 ± 0.06 (7 ± 3%)	0.51 ± 0.14 (15 ± 5%)	7.54 ± 2.07 (10 ± 2%)
Fuzzy Logic	1	0.10 (5%)	0.48 (13%)	8.54 (11%)

Table 3.5. NRMSEs of responses of closed-loop control system

3.4.3 Parameter-randomized In-silico Controller Testing

In order to further examine the performance of each controller, we also randomly varied the parameters in the identified model and applied to the controller to see if the controller is still able to bring MAP back to normal level. Before perturbing the parameters, we varying one parameter at a time to justify how much range we can perturb of each parameter. As the results of this one-parameter perturbation, we can define ±15% of the nominal value is suitable range for random perturbation since all the parameters within this range can always reproduce reasonable responses, like MAP response is always within its reasonable range. One example result of each controller are shown in the Figure 3.4.

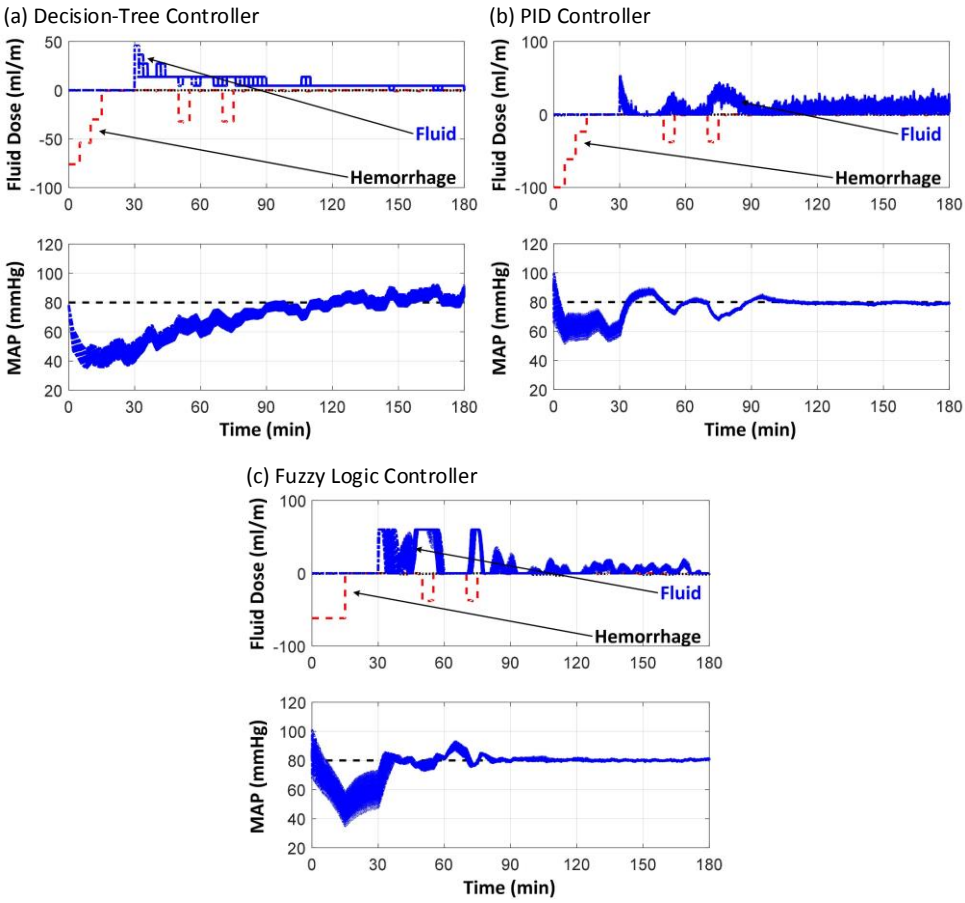

Fig.3.4. Input profiles and MAP responses of closed-loop feedback control system with parameter-randomized model

The results of parameter-randomized in-silico controller testing were also compared with different criterion, including RMSE, NRMSE, median prediction error (MDPE), median absolute performance error (MDAPE), divergence (DIV), and Wobble [48], and all of them are list in Table 3.6. As the result, we can conclude that the PID and fuzzy logic controllers have better performance to handle hemorrhage problems.

Controller (mean (SD))	DT	PID	Fuzzy Logic
RMSE [mmHg]	19.45 (1.15)	6.92 (0.41)	12.00 (0.90)
NRMSE [·]	0.29 (0.02)	0.09 (0.01)	0.18 (0.02)
MDPE [·]	-2.39 (10.04)	0.36 (0.88)	0.24 (0.06)
MDAPE [·]	10.99 (4.62)	1.38 (0.31)	0.50 (0.13)
DIV [·]	-0.08 (0.10)	-0.08 (0.06)	-0.07 (0.02)
Wobble [·]	6.32 (3.26)	0.86 (0.21)	0.34 (0.11)

Table 3.6. Parameter-randomized in-silico controller testing results

Chapter 4: Sensitivity Analysis

4.1 Overview

A credible mathematical model can enable controller designers to easily obtain insights on system behaviors and investigate the influence of each physiological component on the performance of closed-loop resuscitation controllers via analysis and simulation. Thanks to the power of computation, mathematical models can be evaluated in the forms of in-silico and hardware-in-the-loop test methods, which are efficient ways to test the closed-loop controller if their performance and robustness are sufficient against the wide-range clinical scenarios and the physiological variability. Besides, by varying the parameters in the model to generate random subjects and applying to the non-clinical test methods, the behavior of the controllers under different cases, especially the worst-case, can also be studied. Thus, based on the purpose of establishing validity and utility of the model, in-silico computational simulation incorporating mathematical models is essential for pre-clinical evaluation, which also reduce time and cost in controller testing compare with an animal study or experiment.

In order to examine the validity of the BV-CO-MAP hemodynamic model to see if the model has the potential to contribute the design and evaluation of model-based closed-loop resuscitation controllers, we implemented the same controllers used in the animal experiments and applying them to the BV-CO-MAP model and study the discrepancy between in-silico simulation and experimental dataset in the previous chapter. However, the hemodynamic model consists 11 parameters, which dimension is too high and costs a lot of computation. Besides, based on the characteristics of

physiological-based model and the identification results in previous section, we think some of parameters might depend on each other, which means the model might has over-fitting issue and the variabilities of some group of parameters can eliminated. Thus, parametric sensitivity analysis will also be applied in order to determine high-sensitivity parameters (have a large contribution on the model outputs) and low-sensitivity parameters (have a small contribution on the model outputs). With the sensitivity results, we can further understand the identifiability properties of the model and obtain a lower dimension model by fixing identified low-sensitivity parameters in the model at some certain nominal values to save the computation cost and solve potential over-fitting issue.

After the sensitivity of each parameter had been ranked, we only varied the high-sensitivity parameters to generate random subjects, which the distributions of parameters are based on the identification results and then applied to the controller to do further in-silico controller testing.

4.2 Parametric Sensitivity Analysis

The computational hemodynamic model provides important insights into the underlying mechanism of function of circulatory. However, the parameter estimation in the model might be a challenge due to possibility of model being over-parameterized. Thus, sensitivity analysis also presents a key tool for exploring the identifiability of parameters in the model, which order of parameters is the same as we use in identification section as following:

$$X = \{\alpha_u, \alpha_v, K_p, \theta_1, \theta_2, \theta_3, \theta_4, \theta_5, k, p, MAP_{target}\}$$

In this section, local and global sensitivity analyses were performed on the BV-CO-MAP hemodynamic model to determine the relative importance of each parameter or groups of parameters. The goal of this section is to fix identified low-sensitivity parameters at their nominal values and obtain a well-conditioned model which can reduce the issue of over-fitting.

4.2.1 Local Sensitivity Analysis

The 'local' sensitivity analysis (LSA) is the type of sensitivity analysis that can only address the sensitivity relative to the chosen parameter sets and not for the entire feasible parameter space [49]. Since practical reasons that the model in this thesis is complex and hard to apply the differential sensitivity analysis, the one-at-a-time (OAT) method was applied to the LSA of this model, which is the simplest method that repeatedly varies one parameter at a time while holding the others fixed at their nominal values [50]. With this sensitivity analysis method, a sensitivity ranking can be obtained rapidly by varying a parameter by some given percentage while leaving all other parameters constant and then qualifying the contribution of each parameter in model output.

With using the subject-specific optimum of each optimization as the reference point of parameter set we want to estimate, we varied the parameters by -20%, -15%, -10%, -5%, 5%, 10%, 15%, and 20% with OAT method and monitored the changes in BV, CO, and MAP responses. One example results of LSA are shown in Figure 4.1.

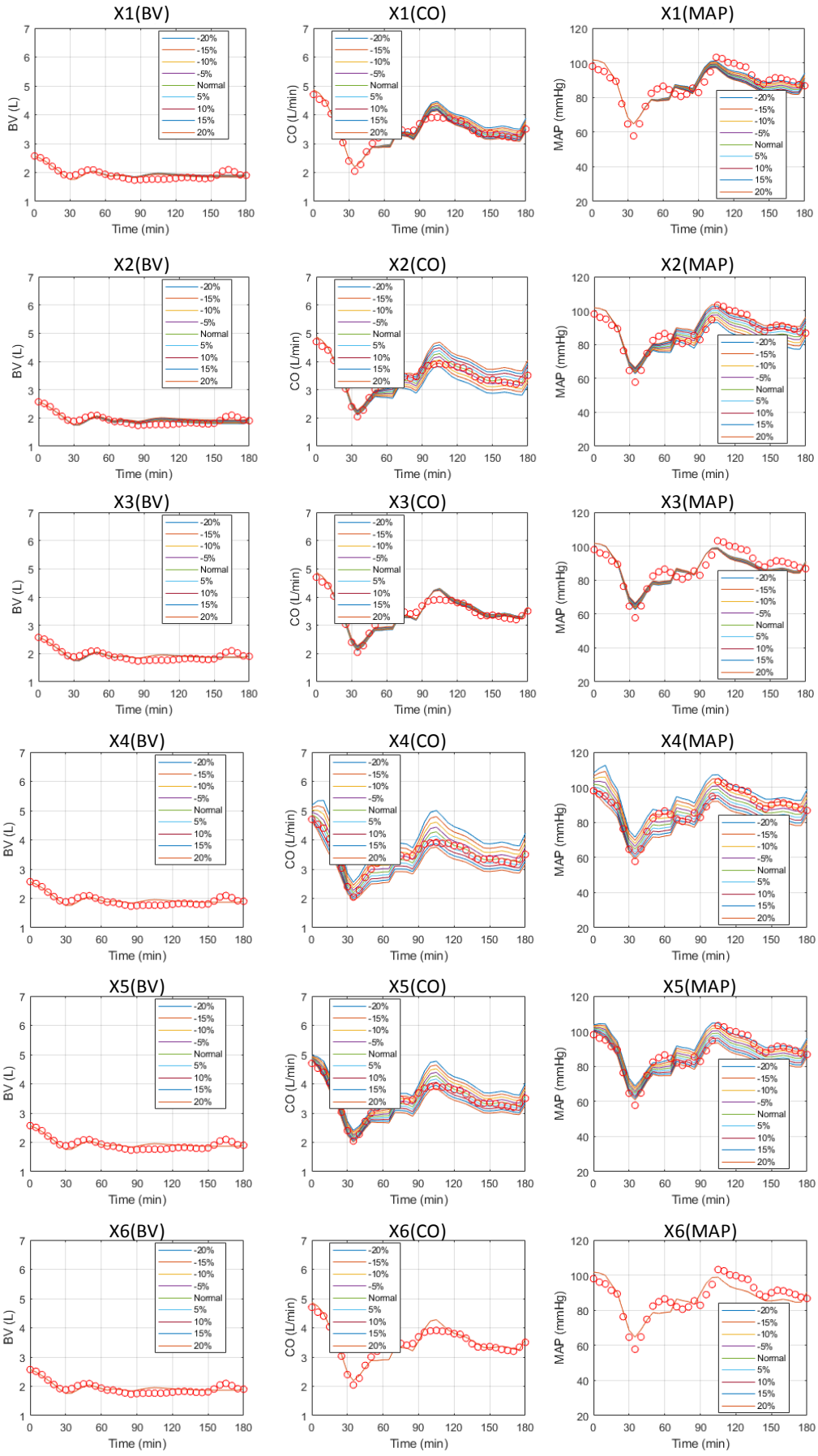
X1(BV)
X1(CO)
X1(MAP)
X2(BV)
X2(CO)
X2(MAP)
X3(BV)
X3(CO)
X3(MAP)
X4(BV)
X4(CO)
X4(MAP)
X5(BV)
X5(CO)
X5(MAP)
X6(BV)
X6(CO)
X6(MAP)
BV (L)
CO (L/min)
MAP (mmHg)
Time (min)
-20%
-15%
-10%
-5%
Normal
5%
10%
15%
20%

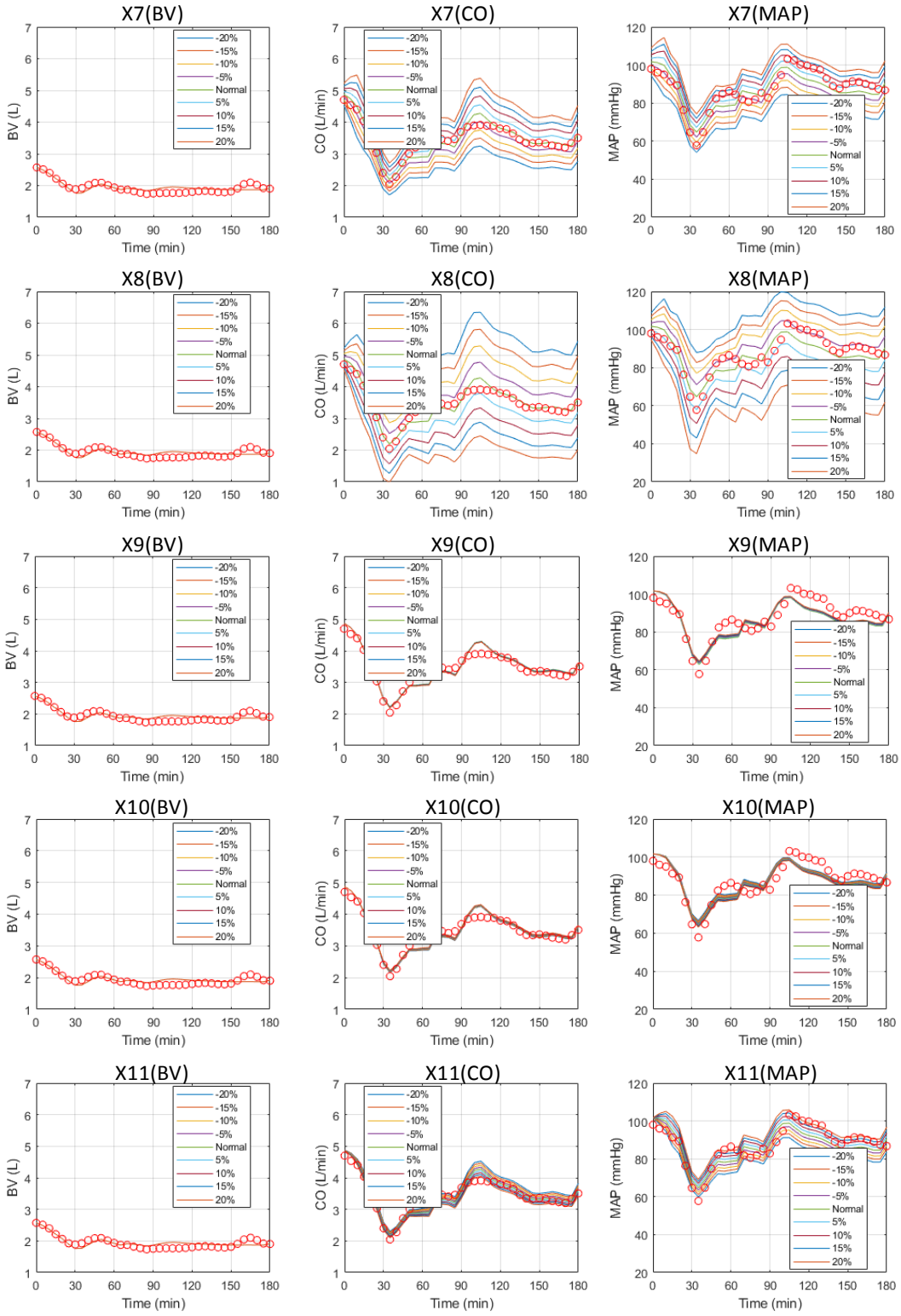

Fig. 4.1. Local Sensitivity Results

From the LSA results of all 11 subjects, we can note that the four parameters in the CO sub-model ($X_{4,5,7,8}$), which are $\{\theta_1, \theta_2, \theta_4, \theta_5\}$, have high sensitivity compare to the rest of parameters, especially the X_7 and X_8 (θ_4 and θ_5) are high sensitivity parameters in all 11 LSA results of subjects.

4.2.2 Global Sensitivity Analysis

Despite the simplicity of OAT local sensitivity method however, this approach did not fully explore the input parameter space. Besides, since this method did not vary input parameters simultaneously, the OAT approach also cannot detect the effects of interaction between input variables. Thus, based on these reasons, the 'global' sensitivity analysis (GSA) was also performed to the BV-CO-MAP hemodynamic model.

The GSA explores parameter space so that it provides robust sensitivity measures in the presence of nonlinearity and interactions among the parameters in the model [51]. While the OAT method mentioned in previous section is different-based, one of the most popular GSA forms called Sobol' method is based on decomposition of the model output variance into the summands of variances of the input parameters in increasing dimensionality [52]. Sobol sensitivity analysis (SSA) determines the contribution of each input variable and their interactions to the overall model output variance. Thus, SSA is used to identify key parameters whose uncertainty most affects the variation of the model output of interest, especially for the models that are nonlinear and complex.

However, most models in reality are involving inequality constraints, such as some parameters in the model are dependent, which implies that the shape of the parameter space may no longer be hyper-rectangle, which the shape is only determined

by the upper and lower bounds of each parameter. In the BV-CO-MAP hemodynamic model, we imposed minimum and maximum thresholds for the model output since BV, CO and MAP should vary in reasonable ranges, which can be defined as inequality constraints. Thus, because the SSA problem in the thesis is defined in a non-rectangular domain, the acceptance-rejection sampling method (ARS) is implied to the SSA to deal with non-rectangular parameter space problem [53]. By replacing the probability distribution function (pdf) in the calculation of model output variance, the Sobol indices can be transformed to the parameter space with any shape or disconnected cases. After the Sobol indices are calculated, we can rank the eleven parameters to find out which parameters are important for different states.

As shown in Figure 4.2, the joint pdf, $p(y,z)$, where y is the arbitrary subset of variables, z is the complementary subset of variables, and (y,z) is the whole parameter set input of the model, is in the absence of constrain in a rectangle domain, H^n, where n is the number of dimensions. By assuming that the constraining the variables to an area $\Omega^n \subset H^n$ and labeling the points inside the Ω^n as 1, while the points outside the Ω^n as 0, the $I^{\Omega}(y,z)$ can be defined as follows:

$$I^{\Omega}(y,z) = \begin{cases} 1, & (y,z) \in \Omega^n \\ 0, & (y,z) \notin \Omega^n \end{cases} \tag{4.1}$$

With similar setting mentioned above, we can also implies that the modified joint pdf, $p^{\Omega}(y,z)$, which takes zero values in the region outside of Ω^n, is proportional to $p(y,z)$ within Ω^n, and can be written as:

$$p^{\Omega}(y,z) = \begin{cases} \frac{p(y,z)}{\bar{I}}, & (y,z) \in \Omega^n \\ 0, & (y,z) \notin \Omega^n \end{cases} \tag{4.2}$$

where $\bar{I}$ is a scaling factor that represents the ratio of volume between Ω^n and H^n,

which can be written as:

$$\bar{I} \approx \frac{1}{N}\sum_{i=1}^{N} I^{\Omega}(y_i, z_i) \tag{4.3}$$

where N is total sample size for calculating the sensitivity, and the accuracy of $\bar{I}$ can be increased by increasing N.

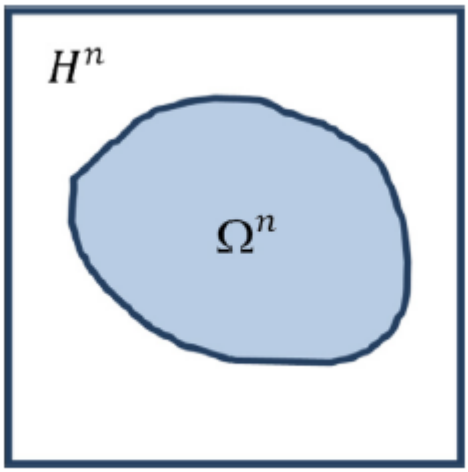

Fig. 4.2. Domain $\Omega^n \subset H^n$ [54]

With modifying Monte Carlo (MC) numerical estimator [54] in the original SSA method and applying $I^{\Omega}(y_i, z_i)$ from the Equation (4.1), the expect value, f_0, and total variance, D, of the model output are computed using the modified MC estimators, and which can be written as:

$$f_0 \approx \frac{1}{IN}\sum_{i=1}^{N} f(y_i, z_i) I^{\Omega}(y_i, z_i) \tag{4.4}$$

$$D \approx \frac{1}{IN}\sum_{i=1}^{N} [f(y_i, z_i) - f_0]^2 I^{\Omega}(y_i, z_i) \tag{4.5}$$

where $f(y_i, z_i)$ is the model output with the input variables (y_i, z_i).

In order to calculate Sobol sensitivity indices, the constrained marginal pdf needs to be defined before the calculation, which represents the pdf that only varying group of specific parameters, and can be written as:

$$p^{\Omega}(y_j) \approx \frac{1}{\bar{I}N_z}\sum_{k=1}^{N_z} I^{\Omega}(y_{jk}, z_{jk}) \tag{4.6}$$

where N_z is sample size for calculating the constrained marginal pdf.

For the Sobol sensitivity indices, there are two different indices to represent the sensitivity of the parameters in the model. One of the indices is the main effect index of the subset y, S_y, which represents the first order sensitivity of the subset y. The other index is the total effect index of the subset y, S_y^T, which represents the interaction between the subset y and the other parameters. Besides, based on the knowledge of Sobol indices [52], we also know that the main effect index of the subset y, S_y, and the total effect index of the subset z (complementary subset), S_z^T, cover all the contribution of the model output. Thus, the relationship between S_y and S_z^T can be defined as:

$$S_y + S_z^T = 1 \tag{4.7}$$

For the ARS method, we can apply the values from the Equation (4.3), (4.4), (4.5) and (4.6) to the equation of the total effect index of the subset z, S_z^T, which is written as follows:

$$S_z^T = \frac{1}{2DN\bar{I}^2}\sum_{l=1}^{N}\left[[f(y_l, z_l)I^{\Omega}(y_l, z_l) - f(y_l, z_l')I^{\Omega}(y_l, z_l')]^2\frac{1}{p^{\Omega}(y_l)}\right] \tag{4.8}$$

where the subset z with notation, z_l', is another random complementary parameters subset generated from the (y, z), which fixes y and varies z randomly.

Because we know that the relationship between S_y and S_z^T in the Equation (4.7), the S_y can be derived by plugging in the S_z^T from the Equation (4.8) to the Equation (4.7), which S_y can be expanded as:

$$S_y = 1 - \frac{1}{2DN\bar{I}^2}\sum_{l=1}^{N}\left[[f(y_l, z_l)I^{\Omega}(y_l, z_l) - f(y_l, z_l')I^{\Omega}(y_l, z_l')]^2\frac{1}{p^{\Omega}(y_l)}\right] \tag{4.9}$$

By monitoring the changes of output at different time instants (5 minutes time interval is applied) and using their value to calculate S_y of corresponded time instants, we can examining the time evolution of parametric sensitivity functions, which offers additional insights as to the relative importance and identifiability properties of the parameters in the model.

The sensitivity of 11 parameters in BV, CO, MAP responses of different timeline are ranked and shown in Figure 4.3, which higher value indicates higher ranking (11 in (b) represents highest rank). As the CO and MAP results of Sobol analysis, which contain the contribution from all 11 parameters, we can note that the three parameters in the CO sub-model and one in the MAP sub-model ($X_{4,7,8,9}$), which are $\{\theta_1, \theta_4, \theta_5, k\}$, have high sensitivity compare to the rest of parameters, especially the X_7 (θ_4) are high sensitivity parameters in whole timeline.

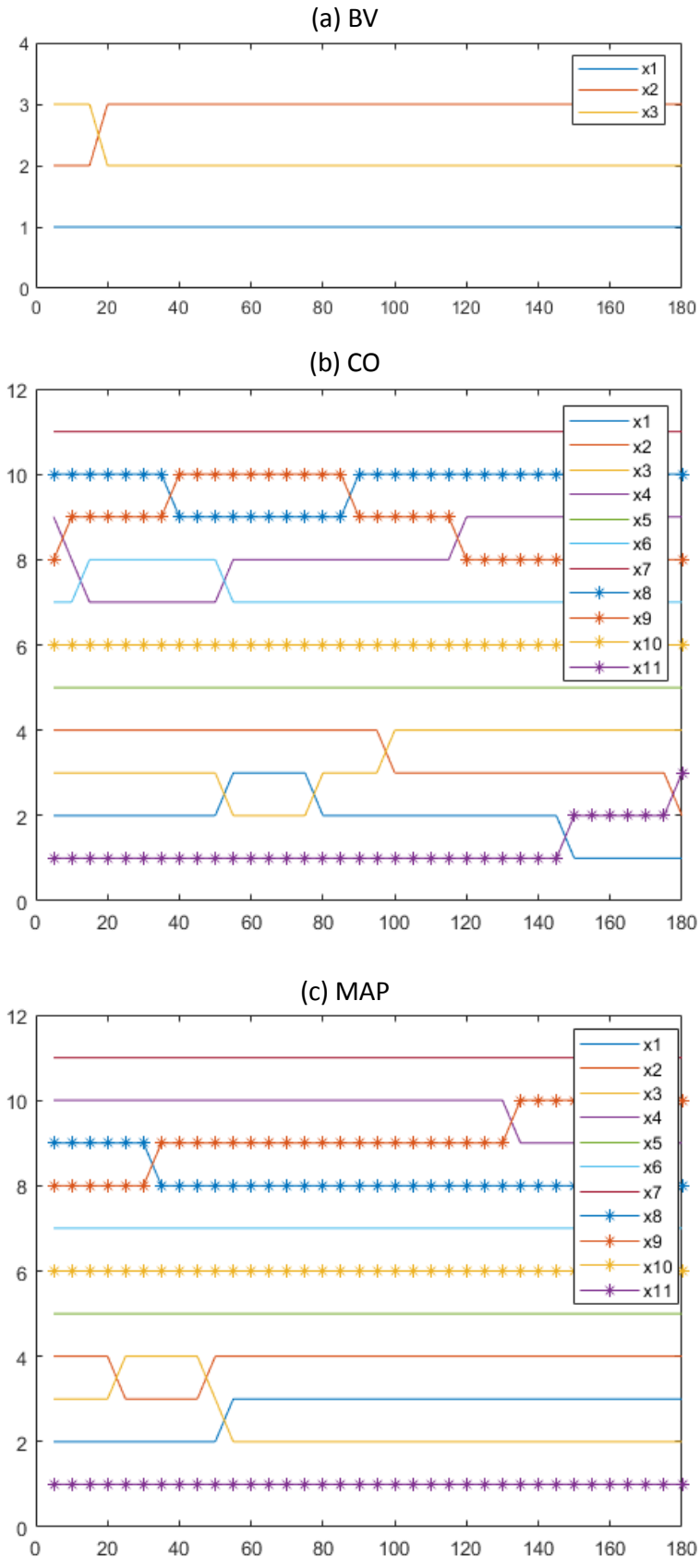

Fig. 4.3. Global sensitivity ranking

Chapter 5: Conclusion and Future Work

5.1 Discussion

In this thesis, we have developed a control-theoretic model that can reproduce hemodynamic responses of desired endpoints in clinical practice to fluid infusion or hemorrhage, such as blood volume (BV), stroke volume (SV), cardiac output (CO), total peripheral resistant (TPR), and mean arterial pressure (MAP). Because of the simplicity, the proposed model can become a viable basis for closed-loop resuscitation controller design and evaluation. Besides, the physiological transparency of the proposed model allow credible validation and implementation for controller designer. The accuracy and properties of this proposed model are further discussed specifically in following.

From the results of system identification (Chapter 3), the model accuracy can be determined in terms of the fitting error between measured and model-predicted values. By varying 11 degree of freedom in the model, it can accurately reproduce the hemodynamic responses with individual animals in both crystalloid (LR) and colloid (Hex) fluid infusion cases. Across the open-loop identification (only using input-output data) of all 11 animals, the RMSEs associated with BV, CO, and MAP were 0.09 ± 0.04 L (crystalloid) and 0.09 ± 0.04 L (colloid), 0.25 ± 0.10 Lpm (crystalloid) and 0.21 ± 0.07 Lpm (colloid), 6.10 ± 1.81 mmHg (crystalloid) and 6.07 ± 1.47 mmHg (colloid), respectively (Table 3.2). Comparing the results with previous version of hemodynamic model, the goodness of current version is that MAP sub-model can reproduce the TPR term and feedback to CO sub-model in order to give us insight of how blood vessel

muscles change in cardiac regulation system, which also enhance the physiological transparency, and perform better fitting which can be observed in the CO and MAP responses. Besides, after we applied different experimental-used controllers and consider closed-loop control system, the system can also reproduce similar results to the experimental data. Overall, the proposed model exhibited remarkable performance in reproducing hemodynamic responses its simple model structure, which might offer a more viable basis in the field of model-based controller design than complex first-principles models.

For the parametric sensitivity discussed in the Chapter 4, the time evolution of the parametric sensitivity provide further insights of the relative importance and identifiability of the model parameters. Although the controller had been examined in the randomize all 11 parameters in the model with certain range, the model still need sensitivity analysis to find out if there is a group of parameters which are dependent to each other and the rule of generating random subjects should be based on this result. From the rankings of the parameters in both local and global sensitivity analysis, while some parameters has similar ranking pattern in both method (High sensitivity: θ_1, θ_4 and θ_5; Low sensitivity: θ_2 and p), other rankings of parameters produce more distinct pattern. This observation might occurs because (a) local sensitivity is a subject-specific analysis that parametric sensitivity is restricted with certain region in parameter space or (b) the acceptance-rejection sampling method decrease the accuracy of global sensitivity (Sobol), which needs much more model samples to investigate all the parameter space. Despite the parameters with distinction, the other parameters with similarity in both methods can be conclude that they have high (low) sensitivity in all

feasible domain of parameter space, which we can fix the low sensitivity parameters and vary other parameters, especially high sensitivity parameters, to generate random subjects.

5.2 Future Work

There are some aspects of the model can be potentially improved in future to make the proposed model more amenable to the closed-loop fluid resuscitation controller design and evaluation. Since parametric sensitivity analysis of both methods are not identical, the parametric sensitivity should be further studied by calculating correlation coefficients of each parameter as well as increase the sampling number in Sobol analysis to enhance accuracy. Besides, after the parameters have been ranked and fixed the low-sensitivity parameters as their nominal value, the model with lower dimensions should re-identified to fit the dataset and see if the partial parameters (exclude low-sensitivity parameter) can make the model still adapt to all specific subjects. Then in-silico closed-loop controller testing can be also applied to this partially individualized model in order to obtain a better-conditioned model which can deal with issues in clinical practice, such as physiologically variability and challenging clinical scenarios, with higher efficiency.

For the model structure standpoint, the current model for the controller evaluation is assumed that the heart rate (HR) and urine output (UO) information is available as input to the model. However, the heart rate and urine measurements in some clinical cases might not be available, and an ideal model should generate all the desired responses itself. Thus, the heart rate component of baroreflex system and kidney

function for urine output will be incorporated in future hemodynamic model, which mechanism of HR might be similar to the mechanism of changing TPR in the MAP sub-model. In addition, the unstressed blood volume in the current model is set to be a constant, while the regulation of unstressed blood volume might be also an important component in hemodynamic responses to blood volume perturbation [55]. Based on these ideas, the expansion of the updated model may potentially facilitate the creation of physiological models suited to design and evaluation of closed-loop controllers in the field of physiological system.

5.3 Conclusion

The proposed control-theoretic hemodynamic model was developed and analyzed with experiment dataset, which results show that the model can be beneficial for the design and evaluation of closed-loop feedback fluid resuscitation system in critically ill patients. The proposed model was equipped with several characteristics, including structural simplicity, physiological transparency, and predicted accuracy, which are essential for in-silico testing and model-based pre-clinical evaluation. As the result, a wide range of clinical scenarios can be evaluated via rigorous in-silico testing methods, especially the worst case of closed-loop fluid resuscitation controllers' behavior. Besides, since all the analysis and evaluation can be done within computational programming, the in-silico simulations incorporating credible models potentially reduce time and cost of controller design compare with the large-scale animal study. Ultimately, the efforts we made into investigating and improving the hemodynamic model so far is impactful to the autonomous fluid resuscitation and critical care

monitoring systems.

Bibliography

[1] Salinas, J., Drew, G., Gallagher, J., Cancio, L. C., Wolf, S. E., Wade, C. E., Holcomb, J. B., Herndon, D. N., and Kramer, G. C., 2008, "Closed-loop and decision-assist resuscitation of burn patients," J. Trauma, **64**(4), pp. S321-332.

[2] Hoskins, S. L., Elgjo, G. I., Lu, J., Ying, H., Grady, J. J., Herndon, D. N., and Kramer, G. C., 2006, "Closed-loop resuscitation of burn shock," J. Burn Care Res. Off. Publ. Am. Burn Assoc., **27**(3), pp. 377–385.

[3] Rinehart, J., Lee, C., Cannesson, M., and Dumont, G., 2013, "Closed-loop fluid resuscitation: robustness against weight and cardiac contractility variations," Anesth. Analg., **117**(5), pp. 1110–1118.

[4] Ying, H., and Sheppard, L. C., 1990, "Real-time expert-system-based fuzzy control of mean arterial pressure in pigs with sodium nitroprusside infusion," Med. Prog. Technol., **16**(1–2), pp. 69–76.

[5] Nise, N. S., 2011, Control Systems Engineering, John Wiley & Sons, Inc., NJ, USA.

[6] Skogestad, S., and Postlethwaite, I., 2005, Multivariable Feedback Control: Analysis and Design, John Wiley & Sons, Ltd, West Sussex, UK.

[7] Slotine, J.-J., and Li, W., 1991, Applied Nonlinear Control, Pearson, N.J, USA.

[8] Khalil, H. K., 2001, Nonlinear Systems, Pearson, N.J, USA.

[9] Ioannou, P., and Sun, J., 2012, Robust Adaptive Control, Dover Publications, NY, USA.

[10] Rafie, A. D., Rath, P. A., Michell, M. W., Kirschner, R. A., Deyo, D. J., Prough, D. S., Grady, J. J., and Kramer, G. C., 2004, "Hypotensive resuscitation of multiple hemorrhages using crystalloid and colloids," Shock Augusta Ga, **22**(3), pp. 262–269.

[11] Chaisson, N. F., Kirschner, R. A., Deyo, D. J., Lopez, J. A., Prough, D. S., and Kramer, G. C., 2003, "Near-infrared spectroscopy-guided closed-loop resuscitation of hemorrhage," J. Trauma, **54**(5 Suppl), pp. S183-192.

[12] Elgjo, G. I., Traber, D. L., Hawkins, H. K., and Kramer, G. C., 2000, "Burn resuscitation with two doses of 4 mL/kg hypertonic saline dextran provides sustained fluid sparing: a 48-hour prospective study in conscious sheep," J. Trauma, **49**(2), pp. 251-263-265.

[13] Lewis, F. R., 1986, "Prehospital intravenous fluid therapy: physiologic computer modelling," J. Trauma, **26**(9), pp. 804–811.

[14] Wears, R. L., and Winton, C. N., 1990, "Load and go versus stay and play: analysis of prehospital i.v. fluid therapy by computer simulation," Ann. Emerg. Med., **19**(2), pp. 163–168.

[15] Mardel, S. N., Simpson, S. H., Kelly, S., Wytch, R., Beattie, T. F., and Menezes, G., 1995, "Validation of a computer model of haemorrhage and transcapillary refill," Med. Eng. Phys., **17**(3), pp. 215–218.

[16] Simpson, S. H., Menezes, G., Mardel, S. N., Kelly, S., White, R., and Beattie, T., 1996, "A computer model of major haemorrhage and resuscitation," Med. Eng. Phys., **18**(4), pp. 339–343.

[17] Abram, S. R., Hodnett, B. L., Summers, R. L., Coleman, T. G., and Hester, R. L., 2007, "Quantitative Circulatory Physiology: an integrative mathematical model of human physiology for medical education," Adv. Physiol. Educ., **31**(2), pp. 202–210.

[18] Kofránek, J., and Rusz, J., 2010, "Restoration of Guyton´s diagram for regulation of the circulation as a basis for quantitative physiological model development," Physiol. Res., **59**(6), pp. 897–908.

[19] Pirkle, J. C., and Gann, D. S., 1976, "Restitution of blood volume after hemorrhage: role of the adrenal cortex," Am. J. Physiol., **230**(6), pp. 1683–1687.

[20] Hedlund, A., Zaar, B., Groth, T., and Arturson, G., 1988, "Computer simulation of fluid resuscitation in trauma. I. Description of an extensive pathophysiological model and its first validation," Comput. Methods Programs Biomed., **27**(1), pp. 7–21.

[21] Arturson, G., Groth, T., Hedlund, A., and Zaar, B., 1989, "Computer simulation of fluid resuscitation in trauma. First pragmatic validation in thermal injury," J. Burn Care Rehabil., **10**(4), pp. 292–299.

[22] Carlson, D. E., Kligman, M. D., and Gann, D. S., 1996, "Impairment of blood volume restitution after large hemorrhage: a mathematical model," Am. J. Physiol., **270**(5 Pt 2), pp. R1163-1177.

[23] Bighamian, R., Reisner, A. T., and Hahn, J. O., 2016, "A lumped-parameter subject-specific model of blood volume response to fluid infusion," Front. Physiol., **7**(Article 390).

[24] Guyton, A. C., Taylor, A. E., and Granger, H. J., 1975, Dynamics and control of the body fluids, W.B. Saunders.

[25] Beard, D. A., and Feigl, E. O., 2011, "Understanding Guyton's venous return curves," Am. J. Physiol. Heart Circ. Physiol., **301**(3), pp. H629-633.

[26] Young, D. B., 2010, Control of Cardiac Output, Morgan & Claypool Life Sciences, CA, USA.

[27] Sagawa, K., Maughan, W. L., Suga, H., and Sunagawa, K., 1988, Cardiac Contraction and the Pressure-volume Relationship, Oxford University Press.

[28] Santamore, W. P., and Burkhoff, D., 1991, "Hemodynamic consequences of ventricular interaction as assessed by model analysis," Am. J. Physiol., **260**(1 Pt 2), pp. H146-157.

[29] Morley, D., Litwak, K., Ferber, P., Spence, P., Dowling, R., Meyns, B., Griffith, B., and Burkhoff, D., 2007, "Hemodynamic effects of partial ventricular support in chronic heart failure: results of simulation validated with in vivo data," J. Thorac. Cardiovasc. Surg., **133**(1), pp. 21–28.

[30] Uemura, K., Kawada, T., Kamiya, A., Aiba, T., Hidaka, I., Sunagawa, K., and Sugimachi, M., 2005, "Prediction of circulatory equilibrium in response to changes in stressed blood volume," Am. J. Physiol. Heart Circ. Physiol., **289**(1), pp. H301-307.

[31] Montani, J.-P., and Van Vliet, B. N., 2009, "Understanding the contribution of Guyton's large circulatory model to long-term control of arterial pressure," Exp. Physiol., **94**(4), pp. 382–388.

[32] Coleman, T. G., and Guyton, A. C., 1969, "Hypertension caused by salt loading in the dog," Circ. Res., **25**(2), pp. 153–160.

[33] Fowler, A. C., and McGuinness, M. J., 2005, "A delay recruitment model of the cardiovascular control system," J. Math. Biol., **51**, pp. 508-526.

[34] Cavalcanti, S., 2000, "Arterial baroreflex influence on heart rate variability: a mathematical model-based analysis," Med. Biol. Eng. Comput., **38**(2), pp. 189-197.

[35] Hammer, P. E., and Saul, J. P., 2005, "Resonance in a mathematical model of baroreflex control: arterial blood pressure waves accompanying postural stress," Am. J. Physiol. Regul. Integr. Comp. Physiol., **288**, pp. R1637-1648.

[36] Ottesen, J. T., 1997, "Modelling of the baroreflex-feedback mechanism with time-delay," J. Math. Biol., **36**, pp. 41-63.

[37] Ottesen, J. T., Olufsen, M. S., and Larsen, J. K., 2004, "Applied Mathematical Models in Human Physiology," SIAM Monographs on Mathematical Modelling and Computation.

[38] Liu, H.-K., Guild, S.-J., Ringwood, J. V., Barrett, C. J., Leonard, B. L., Nguang, S.-K., Navakatikyan, M. A., and Malpas, S. C. 2002, "Dynamic baroreflex control of blood pressure: influence of the heart vs. peripheral resistance," Am. J. Physiol. Regulatory Integrative Comp. Physiol., **283**, pp. R533-542.

[39] Malpas, S. C., 2002, "Neural influences on cardiovascular variability: possibilities and pitfalls," Am. J. Physiol. Heart Circ. Physiol., **282**, pp. H6–20.

[40] Ringwood, J. V., and Malpas, S. C., 2001, "Slow oscillations in blood pressure via a nonlinear feedback model," Am. J. Physiol. Regulatory Integrative Comp. Physiol., **280**, pp. R1105–1115.

[41] Atlas, S. A., 2007, "The renin-angiotensin aldosterone system: pathophysiological role and pharmacologic inhibition, J. Manag. Care Pharm., **13**(8 Suppl. B), pp. 9-20.

[42] Kletting, P., and Glatting G., 2009, "Model selection for time-activity curves: The corrected Akaike information criterion and the F-test," Z. Med. Phys., **19**, pp. 200-206.

[43] Marques, N. R., Ford, B. J., Khan, M. N., Kinsky, M., Deyo, D. J., Mileski, W. J., Ying, H., and Kramer, G. C., 2017, "Automated closed-loop resuscitation of multiple hemorrhages: a comparison between fuzzy logic and decision table controllers in a sheep model," Disaster Mil. Med., **3**:1.

[44] Vaid, S. U., Shah, A., Michell, M. W., Rafie, A. D., Deyo, D. J., Prough, D. S., and Kramer, G. C., 2006, "Normotensive and hypotensive closed-loop resuscitation using 3.0% NaCl to treat multiple hemorrhages in sheep," Crit. Care Med., **34**(4), pp. 1185–1192.

[45] Henschen, S., Busse, M. W., Zisowsky, S., and Panning, B., 1993, "Determination of plasma volume and total blood volume using indocyanine green: a short review," J. Med., **24**(1), pp. 10–27.

[46] Bighamian, R., Parvinian, B., Scully, C. G., and Kramer, G., 2018, "Control-oriented physiological modeling of hemodynamic responses to blood volume perturbation," Control Eng. Pract., **73**, pp.149-160.

[47] The Mathworks, Inc. (2017) Documentation on optimization toolbox. [Online]. Available: https://www.mathworks.com/help/pdf_doc/optim/optim_tb.pdf

[48] Varvel, J. R., Donoho, D. L., and Shafer, S. L., 1991, "Measuring the predictive performance of computer-controlled infusion pumps," J. Pharmacokinet. Biopharm., **20**(1), pp. 63-94.

[49] Hamby, D. M., 1994, "A review of techniques for parameter sensitivity analysis of environmental models," Environmental Monitoring and Assessment, **32**, pp. 135-154.

[50] Gardner, R. H., Huff, D. D., O'Neill, R. V., Mankin, J. B., Carney, J., and Jones, J., 1980, "Application of Error Analysis to a Marsh Hydrology Model," Water Resource Res., **16**, pp. 659-664.

[51] Looss, B., Lemaître, P., 2015, "A Review on Global Sensitivity Analysis Methods," Uncertainty Management in Simulation-Optimization of complex Systems, **59**, pp. 101-122.

[52] Sobol, I. M., 2001, "Global sensitivity indices for nonlinear mathematical models and their Monte Carlo estimates," Mathematics and Computers in Simulation, **55,** pp. 271-180.

[53] Kucherenko, S., Klymento, O. V., and Shah, N., 2017, "Sobol' indices for problems defined in non-rectangular domains," Reliability Engineering and System Safety, **167**, pp. 218-231.

[54] Sobol, I. M., 1998, "On quasi-Monte Carlo integrations," Math. Comput. Simulation, **47**(2-5), pp. 52-61.

[55] Costanzo, L. S., 2014, Physiology (5^{th} ed.), Elsevier Health Sciences.